Process simulation of ammonia synthesis over optimized Ru/C catalyst and multibed Fe + Ru configurations

Antonio Tripodi, Matteo Compagnoni, Elnaz Bahadori, Ilenia Rossetti*

Chemical Plants and Industrial Chemistry Group, Dip. Chimica, Università degli Studi di Milano, INSTM Unit Milano-Università and CNR-ISTM, via C. Golgi, 19, I-20133 Milano, Italy

Abstract

Ammonia synthesis over different Iron- and Ruthenium-based catalysts was modelled with appropriate rate models, used for the simulation of the process under different configurations and conditions. The kinetic models have been simulated and validated against experimental data. A scaled up reactor has been designed, at first with a once through configuration. On this model reactor we performed a sensitivity analysis to optimise the reaction conditions. Then, the sizing of an ammonia separation unit and the optimisation of the recycle loop allowed to compare different possible configurations.

A multibed catalytic reactor with intercooling was then designed, using the same catalyst or different catalyst types properly to maximise the ammonia productivity. In particular, Fe-based catalysts were followed by the Ru/C one, in order to push the ammonia productivity towards the equilibrium value.

The goal of the work is the design of an ammonia synthesis loop which couples different catalysts towards the optimisation of productivity and cost of operation and installation

* Corresponding author: ilenia.rossetti@unimi.it – fax: +39-02-50314300

Keywords: Ammonia synthesis; Reactor modelling; Multibed catalytic reactors; Aspen Plus simulation; Kinetic modelling; Temkin equation.

1. Introduction

The production of sufficient food to sustain the huge growth of the world population, mainly in developing countries and newly industrialized ones, represents one of the priorities of the international community. This trend relates to the rising expectations of better living standards, that lead to a higher food demand. A study on food production relative to the most populated country, China, established a linear proportionality between food production and chemical fertilizer production [1] and a similar trend can be observed for India [2]. Generally, chemical fertilizers market dominates also in the developed northern countries, especially in central United States, Canada and Europe [3]. Nowadays, fertilizers production is centralized and the core of the process is constituted by ammonia synthesis. The latter is mainly accomplished through the well known Haber-Bosch process [4] on a plant scale of 1,000 ton/day (100 million tons per year worldwide). This technology represents also the major success of heterogeneous catalytic process used on a large scale [5,6].

Ammonia synthesis is a complex heterogeneous catalytic process, where N_2, H_2 and NH_3 adsorption/desorption on catalyst surface are fundamental steps. Although the underlying chemistry is relatively well known [7,8], very demanding operating conditions for pressure and temperature are needed. For this reason, the technology is very sophisticated and its study continued during the last century, both in the scientific and industrial communities. Iron based catalyst can be used at 150-250 bar and 380-520°C [9], they are sufficiently active and not expensive, but the maximum conversion achievable is limited by inhibition by ammonia. The research to decrease the operating pressure is still in progress [10–14], relying basically on the search of more active materials. The process includes specifically designed reactors, where a multibed configuration is the most employed. For instance,

with traditional Fe-magnetite 4 beds of catalyst, with inter-cooling after each pass lead to a conversion rate up to 15% and a recycling mechanism to achieve up to 98% conversion.

Ruthenium showed higher activity than Fe for ammonia production and it is not inhibited by the product, is as sensitive as Fe to oxygen-containing impurities, but it is less sensitive to sulphur [15,16].

The industrial application of Ru on graphitized carbon was achieved in the Kellogg's Advanced Ammonia Process (KAAP). This process is active in seven world-scale plants, each producing *ca.* 2,000 tonnes per day of ammonia [17] using a "low pressure" synthesis loop operating down to 90 bar. The Ru catalyst is placed in different fixed beds and the higher activity of Ru allows lower operating pressure than Fe. The main drawbacks of Ru/C catalysts are *i)* their inhibition by hydrogen, which prompts for the use of understoichiometric reaction conditions and *ii)* the poor carbon resistance towards methanation, which is catalysed by Ru itself and may corrode the support promoting catalyst sintering and deactivation [18].

Aspen Plus© process simulator has been effectively used to investigate high pressure processes, such as methanol synthesis [19,20], coal gasification [21], biomass gasification [22], Fischer-Tropsch synthesis [23], partial oxidation of natural gas [24]. A basic requirement for a reliable simulation of reactive systems, is the availability of appropriate kinetic equations [25]. Surprisingly, only few authors tried to simulate the ammonia synthesis process implementing detailed and up-to-date kinetic expressions. Yu et al. tried to implement the kinetic parameters of ammonia synthesis for the evaluation of a coal-based polygeneration process to coproduce synthetic natural gas and ammonia [26], but with insufficient detail on kinetics to be reproduced. The control structure design for an ammonia synthesis process was reported by Araujo and Skogestad [27], the reaction kinetics being based on the Temkin–Pyzhev expression. On the other hand, Arora and co-workers investigated small scale ammonia production from biomass [28], but using Gibbs and equilibrium reactors were used to model the ammonia converter. Ammonia production via integrated biomass gasification was also

studied by Andersson and Lundgren [29]. Also in this case the reactor was simulated using a Gibbs reactor, with an iron catalyst.

Neglecting the kinetics, the overall process can still be designed relying on the mass-balances, only, but optimal operating conditions cannot be safely identified, nor the reactors sized, since for this reaction kinetics and thermodynamics obey to opposite requirements.

Therefore this paper proposes the simulation of a relatively low pressure ammonia synthesis reactor (below 120 bar). The kinetic description of the process was based on an original kinetic model, derived on a patented promoted Ru/C catalyst, obtained as a result of 20 years of research in our laboratory: the model was developed in a previous investigation, modifying the Temkin equation with the addition of H_2 and NH_3 adsorption terms, in order to consider their possible concurrent inhibiting effect [30]. The full details on catalyst properties and its performance under industrially relevant conditions can be found elsewhere [31–33]. Temperatures below 500°C are suitable for carbon supported catalysts, preventing the methanation of the graphitised carbon used as support [30,33,34]. Finally, the preliminary process design was here carried out by comparing a commercial catalyst [35] with advanced, second generation Fe-based catalysts tested previously in our laboratories [31] and both these with our home-developed Ru sample. Different multi-bed arrangements were compared and discussed. To better focus the scope of the paper, we have studied the synthesis section only, since the rest of the ammonia process is consolidated.

The goal of the work is then the design of an ammonia synthesis loop which couples different catalysts towards the optimisation of productivity and cost of operation and installation The body of the paper includes the applicative results whereas the details on the selection of the best thermodynamic package to model the system and computational / convergence issues are reported in the appendix.

2. Modelling and simulation

2.1 Kinetic Formulations

The ammonia synthesis process follows the stoichiometry reported in equation (1).

$$N_2 + 3H_2 \leftrightarrows 2NH_3 \qquad \Delta H^0 = -46 \text{ kJ mol}^{-1} \text{ [17]} \qquad (1)$$

The reaction proceeds through several adsorption and dissociation steps [36]. The related kinetic parameters are complex functions of the surface coverage and structure. The best kinetic equation, as determined by comparison between various rival models, was based on the Temkin one, modified on purpose considering the different features of Ru with respect to Fe. This point is crucial because, as already mentioned, Fe-based catalysts are kinetically inhibited by the strong NH_3 adsorption, while Ru is inhibited by H_2 due to its competitive adsorption with N_2. For this reason, in the denominator of the rate-equation we added an additional term to account for hydrogen adsorption ($K_{H2}(a_{H2})^{0.3}$, as reported in equation (2) [33]:

$$\frac{d\eta}{d\tau} = k\,\lambda(q)\,\frac{\left(a_{N_2}\right)^{0.5}\left[\frac{\left(a_{H_2}\right)^{0.375}}{\left(a_{NH_3}\right)^{0.25}}\right] - \frac{1}{K_a}\left[\frac{\left(a_{NH_3}\right)^{0.75}}{\left(a_{H_2}\right)^{1.125}}\right]}{1 + K_{H_2}\left(a_{H_2}\right)^{0.3} + K_{NH_3}\left(a_{NH_3}\right)^{0.2}} \qquad (2)$$

where K_a represent the equilibrium constant, $d\eta/d\tau$ represented the rate of consumption of the defective reactant in mol h^{-1} dm^{-3}_{cat}, k is the kinetic constant of the direct reaction and a_i the activities of reactants and product. $\lambda(q)$ is a stoichiometric parameter set to 1 or 1.2 when the H_2/N_2 feeding ratio is 3 or 1.5 Adsorption equilibrium constants at the denominator were obtained considering the ΔH_{ads} and ΔS_{ads} for H_2 and NH_3 as reported in (3)-(4) [33]:

$$\log_e K_{H_2} = -\frac{56.9024}{R} + \frac{37656}{RT} \qquad (3)$$

$$\log_e K_{NH_3} = -\frac{34.7272}{R} + \frac{29228}{RT} \qquad (4)$$

The behaviour of the already mentioned iron catalysts was instead modelled without resorting to adsorption terms, with simpler power-law rate laws (equations (5) and (6), respectively from [31,33] and [35]):

$$\frac{d\eta}{d\tau} = k\,\lambda(q)\left[(\mathrm{K_a})^2 \mathrm{a}_{N_2}\left(\frac{{\mathrm{a}_{H_2}}^{2.25}}{{\mathrm{a}_{NH_3}}^{1.5}}\right) - \left(\frac{{\mathrm{a}_{NH_3}}^{0.5}}{{\mathrm{a}_{H_2}}^{0.75}}\right)\right] \quad (5)$$

$$\frac{d\eta}{d\tau} = k\left[(\mathrm{K_a})^2 \mathrm{a}_{N_2}\left(\frac{{\mathrm{a}_{H_2}}^{1.5}}{{\mathrm{a}_{NH_3}}^{1}}\right) - \left(\frac{{\mathrm{a}_{NH_3}}^{1}}{{\mathrm{a}_{H_2}}^{1.5}}\right)\right] \quad (6)$$

2.2 Thermodynamic Analysis

The equilibrium constant was originally calculated according to Gillespie and Beattie as reported elsewhere [8]:

$$\log_{10} K_{eq} = -\frac{59.9024}{R} + \frac{37656}{RT} - 2.691122 * \log_{10} T - 5.519265 * 10^{-5} T + 1.848863 * 10^{-7} T^2 \quad (7)$$

The equilibrium ammonia concentration in stoichiometric mixtures (*i.e.* containing 3 moles of hydrogen per mole of nitrogen) are reported in Figure S3. These preliminary calculation represent the basis in order to overcome the activation energy without depressing the equilibrium condition. The pressure range investigated is relatively narrow and shifted to low values, as in the scope of this work.

Although we focus on the reactor loop in this paper, besides the reactor, at least the gas-ammonia separation stage deserves a similar equilibrium analysis, since also the removal efficiency of the liquefied product affects deeply the overall mass balances. The charts mapping the previsions of a single-stage equilibrium separation are shown in Figure . Notice that the maximum ammonia concentration in the recycle stream cannot be greater than the value determined by the reactor outlet conditions.

2.3 Simulation of the micropilot plant

The kinetic model was validated by simulating the micropilot plant used to derive it. The experimental data for reactor outlet under different operating conditions were reported in the literature and were derived as summarised in the following.

Details about the preparation route of the support, catalyst and activation can be found in the related patent [9] and papers published elsewhere [30]. Briefly, a graphitised carbon was used as support and promoters were added by impregnation from aqueous solutions of hydroxides (K and Cs) or nitrates (Ba), in the optimal amount for obtaining: Ba/Ru = 0.6 (mol/mol), Cs/Ru = 1 (mol/mol), and K/Ru = 3.5 (mol/mol). The Ru content, referred to the final catalyst weight, was 3.2 wt%.

To extend the comparison, a Fe-based benchmark catalyst from magnetite [35] was taken as a reference, and newer commercial materials of magnetite and wustite [31] were considered too.

When compared under the same operating conditions as for temperature (430°C) and pressure (100 bar), GHSV = 30000 h^{-1}, but with optimised H_2/N_2 molar ratio of 1.5 for Ru and 3 for Fe, the Ru/C catalyst overperformed (ca. 15.5 vol% NH_3) both the Fe-based catalyst from magnetite (ca. 8 vol% NH_3) and from wustite (ca. 12.5 vol% NH_3). Thia meand that it is possible to decrease by more than 40% the operating pressure or to achieve more than 40% higher conversion per pass under the same operating conditions. Similar advantages are reported for the commercial KAAP process based on Ru/C catalyst.

A continuous tubular reactor of 9 mm internal diameter, 400 mm long, was adopted to collect the kinetic data, by feeding downflow a reactant gas mixture consisting of hydrogen and nitrogen in different volumetric ratio (3:1 or 1.5:1 v/v), with different Gas Hourly Space Velocity (GHSV) through a catalyst bed of 0.15-0.25 mm particles. The GHSV was defined as the ratio of the inlet volumetric gas flow rate at normal conditions and the volume of the catalyst bed, $Nm^3\ m_{cat}^{-3}\ h^{-1}$. The catalyst was diluted with quartz of the same particle size in ratio catalyst/quartz = 1/22 (v/v), to limit the hot spot across the bed. Before the run the catalyst was activated in situ in a flow of the same reactant gas mixture at 30 bar, 450° C, GHSV = 20,000 h^{-1} for 5 h in the case of the Ru/C catalyst. For Fe-based samples, the temperature was increased by 50 $^{\circ}$ C/h from 25 to 350 $^{\circ}$ C, then by 10 $^{\circ}$ C up to 500 $^{\circ}$ C. The whole activation lasted for 2 days. Activity has been determined by evaluating the volumetric concentration of ammonia in the effluent gas, by bubbling it in an excess

of sulphuric acid (0.1 M) and back-titrating the excess acid with a standardized NaOH solution. The flowsheet of the micropilot plant is reported in Figure S2. Kinetic tests were carried out on the Ru-based catalyst, on the magnetite and wustite Fe-based ones, according to a full experimental design, as detailed elsewhere [31,33].

Aspen Plus© provides a built-in 'LHHW kinetics' for calculating the rate of reactions described with a Langmuir–Hinshelwood–Hougen–Watson (LHHW) model as in our approach. This kinetic model consists of a (dimensioned) 'kinetic factor', a 'driving force' expression (with such dimensions as required to get those of r to match those of k_0) and an adsorption term (dimensionless) as in (8). The reaction occurs in the vapour phase and the reaction rate is based on catalyst weight. The chemical species concur to the driving force with their fugacity f powered by the proper exponents for forward and backward reactions (terms 'for' and 'rev' respectively). This approach was followed, instead of implementing a dedicated reaction calculation algorithm, because the aim of this work is to provide a comparison between the intrinsic kinetics of different catalysts (for whom the built-in Aspen Plus© module is enough), rather than to provide a detailed reactor model (which would require customized rate expressions to address the mass-transport phenomena and axial/radial dispersion models).

$$r = \frac{\left(\mathrm{k}_0\, e^{-E_a/RT}\right)\left(\mathrm{K}_{for}\prod_r f_r^{\nu_r} - \mathrm{K}_{rev}\prod_p f_p^{\nu_p}\right)}{\left(\sum_i \mathrm{K}_i \prod_i f_i^{\nu_i}\right)^e} \qquad (8)$$

The consistency of the optimised parameters was checked by the Arrhenius and Van't Hoff equations, leading to the values reported in Table 1. In order to implement the data in Aspen Plus©, the pre-exponential factor was corrected considering the catalyst density equal to: 0.59 g cm^{-3} (as experimentally determined for the Ru/C material), 2.8 – 2.9 g cm^{-3} (magnetite) and 3.25 g cm^{-3} (wustite). This expression was applied with e=1 for model (2), zero otherwise. Table 1 gives a quick reference to the kinetic and adsorption parameters used during reactor simulation.

The 'RPlug' model was adopted in both isothermal and adiabatic conditions. The Peng-Robinson and Redlich-Kwong equation of states were adopted as thermodynamic models to compute the non-

ideality of the gaseous mixture, yielding results in very good agreement for every single-pass calculations of the ammonia yield. For the calculations involving the closed-cycle synthesis, however, the (modified) Redlich-Kwong-Soave EOS was used (see Supporting Information).

2.4 Simulation of the full scale reactor

To perform a screening of the different catalysts performances under similar reaction conditions, the ammonia synthesis was modelled according to the following criteria (Figure):

- reactants conversion is carried out into 3 beds with intercooling stages;
- the beds thermal conditions – either at constant temperature or duty – were fixed;
- only the reactants loop was modelled, while the synthesis gas feed and the separation sections were omitted, assumed as standardised.

The target yield was set on a ton/day scale (55 kg/h of ammonia every 60 kg/h of fresh stoichiometric gases, plus a small quantity of methane). The gases enter the flowsheet at atmospheric pressure, so to have a rough evaluation of the compression work required by the plant sections upstream, the nominal cycle pressure was set to 100 bar, and the separation section was lumped into a single equilibrium stage at -30 °C, in order to approximately foresee its gross cooling duty. The former assumption on the gas inlet at atmospheric pressure is very conservative, since the steam reforming of natural gas provides compressed hydrogen, but it set as internal comparison and reference.

Despite the configuration simplicity, the single loop contains two highly non-linear blocks (the reactor and the separator) which may compromise the calculation convergence at too low purge fractions. On the other hand, a manual short-cut calculation needs assumption on the single-pass conversion that have to be checked against the actual behaviour of the kinetic model. A purge fraction as high as 1% introduces only minor convergence issues (setting a ‘Broyden’ algorithm, tolerance: 1×10^{-5}), provided the initial recycle mass flow and composition are properly guessed. The reported results are achieved under this latter condition.

3. Results and discussion

3.1 Validation of the kinetic model

The validation of the kinetic model was carried out using directly Aspen Plus©, in order to check in advance the computational consistency of the equation. In general, a good agreement between the experimental and simulation results was obtained for a H_2/N_2 feeding ratio equal to 3, in the whole range of temperature, pressure and space velocity experimentally explored (GHSV = 50,000 - 400,000 h^{-1}, T = 360-430 °C, P = 70-100 bar). Figure exemplifies the results for the test at T = 430 °C, P = 70 bar and H_2/N_2 = 3 (v/v).

For the tests with H_2/N_2 ratio equal to 1.5 (v/v) only the simulation at temperature below 430°C revealed a satisfactory agreement between the simulated ammonia fraction in the reactor outlet gas and the experimental values. In Figure and Figure two examples are reported considering the best and the worst cases respectively.

The maximum discrepancy between the calculated and the experimental values were observed at the highest temperature and lowest space velocity (*i.e.* at highest contact time). This occurs for the most favourable understoichiometric feeding ratios.

The use of a very active catalyst such as the one adopted in this work can significantly reduce the contact time maintaining high ammonia yield. Therefore, a trade off with productivity has to be newly searched for this and the other operating parameters, as follows. A similar validation of the kinetic models for the Fe-based catalysts was also done, not reported for the sake of brevity.

A comparative Table of the performances of Ru-based catalysts is also provided (Table 2). The comparison evidences that very high conversion per pass is achievable with this kind of active phase, with very high productivity attained when high conversion can be maintained at high space velocity. Of course, given the decrease of ammonia concentration at reactor outlet when increasing the space

velocity, this point should be matched with the sizing of the recycle and the relative separation and compression duties.

3.1.a Space velocity and temperature effect

Examples of the relationship between activity and space velocity are shown in Figure 3, Figure and Figure . Increasing space velocity will normally decrease outlet ammonia concentration per pass, but it increases total ammonia production flow rate, thus increasing the recycled flow. The decrease of ammonia concentration in the outlet stream led to a decrease of ammonia in the recycle stream. Moreover, the outlet temperature of the converter was lower due to a lower temperature raise under adiabatic condition. Another important issue was the reduction of energy consumption for cooling the recycle gas. Generally, an economic optimum value of space velocity is calculated for every specified process according to the pressure of the system, the structure of reactor and energy costs. For a low-pressure ammonia synthesis loop, a space velocity in the range of 5,000 –10,000 h^{-1} is commonly chosen, while values between 15,000 and 30,000 h^{-1} or $\geq$ 60,000 h^{-1} are commonly selected for middle and high-pressure systems, respectively, using traditional iron catalysts [37].

Figure compares the ammonia production predicted by the kinetic model for low and high residence times (GHSV = 2.0×10^5 h^{-1} and 0.5×10^5 h^{-1}, respectively) with the predictions of the thermodynamic model calculated using the 'RGibbs' reactor model. This kind of reactor model is used to evaluate the conversion at chemical equilibrium through minimization of the Gibbs free energy of the mixture. The comparison was done for a range of reactor temperatures under isothermal conditions choosing the H_2/N_2 ratio equal to 1.5 (v/v). Ru catalyst, as aforementioned, is preferably operated with understoichiometric ratios because of the inhibition effect of H_2.

The ammonia production increases as the reactor temperature increases, due to kinetic reasons, reaches a maximum at a temperature strictly depending on GHSV (430°C and 465°C for the high and

low contact time, respectively) and then decreases with temperature following the equilibrium conversion. The reaction shows then a transition from a kinetic-limited to an equilibrium-limited regime of operation due to the exothermicity of the reaction (ΔH^0 = -46 kJ mol^{-1}) [17]. Suitable reactor configurations (modelled, in principle, as interconnected isothermal and adiabatic stages), aiming then at keeping a temperature as high as to favour the kinetic, but as low as to remain in a convenient equilibrium regime. The isothermal choice implies the direct heat exchange within the bed, ensuring the proper temperature at the inlet of the reactor and a homogeneous thermal profile along the reactor length. This choice implies the use of multitubular reactor configuration to achieve optimal heat exchange. The second choice is usually more common for the first stages of ammonia reactors [38].

Ammonia volume fraction at the outlet of the reactor predicted by the kinetic model under adiabatic conditions is shown in Figure . The threshold temperatures at which the transition from kinetic to thermodynamic condition occurs, are 355 °C and 400°C for the high and low contact time respectively.

It should be noticed that the Gillespie model predicts a lower ammonia equilibrium conversion than those obtained through minimisation of the Gibbs free energy. The Gillespie equation for K_{eq} was applied by us during the development of our kinetic model, thus it correctly represents the limit towards which our reactor prevision converges.

3.1.b Influence of feed composition

The effect of H_2/N_2 ratio on the activity of the novel Ru/C catalyst is shown in Figure . Temperature was set at 430°C. After the maximum conversion, where a thermodynamic regime governs the process, the ammonia production increases with the increasing of H_2/N_2 ratio as expected. On the other side, the opposite trend in the kinetic regime confirmed the consistency of the kinetic expression for ruthenium catalyst. Indeed, Ru is inhibited by H_2 and, thus, low H_2/N_2 ratios are more advantageous in terms of ammonia conversion with respect to the stoichiometric one. The kinetic

expression considers the competitive adsorption between H_2 and N_2 on the Ru-based catalyst (Eq. (2)).

3.1.c Effect of reaction pressure

In order to study the pressure effect, the lowest value of GHSV considered (0.5×10^5 h^{-1}) was used under isothermal conditions. The simulation results are shown in Figure . The relationship between the ammonia concentration at the outlet and reaction pressure is roughly linear: the higher the pressure, the higher would be the concentration of outlet ammonia.

3.2 Full scale reactor: single-pass performances

The first analysis was made feeding a scaled-up syngas flow to 3 adiabatic reaction beds loaded with commercial iron catalyst, whose kinetics are represented by equation (5) (Wustite) and (6) ('KM' promoted Iron, as per [35] and references therein). The configuration included intercooling exchangers, which imposed the bed inlet temperatures and, at first, was without any recycle (*i.e.* the vapor exiting the separator was entirely purged). As expected, a lower temperature granted higher product yields (Figure), but required more catalyst to reach the maximum conversion. The replacement of the iron-based catalyst with the ruthenium-based one, *i.e.* of expression (5) with expression (2) for the last bed, appreciably improved the reactor performance at low catalytic loads. The same yield of 15 kg/h at low temperature (380 °C) was reached with 20 kg of the Wustite material and 10 kg of the Ruthenium-based one, with respect to 90 kg of iron alone. By contrast, operating at 430 °C half of these loads were needed to reach the maximum conversion allowed by the different equilibrium condition.

3.3 Recirculated Reactor performances

The combination of the kinetic models with the overall mass balances is shown in Figure and Figure for the same catalyst combination tested above. It can be noticed that, at intermediate catalyst load (>5 kg in each bed), the properties of the Ru-based material can improve the ammonia yield even at low temperatures. For example, 20 kg of Ru-based catalyst replacing 20 kg of the Fe-based one in the last two stages, at an inlet temperature of 380 °C and 100 bar, give 58 kg/h of ammonia instead of 52 kg/h, *ca*. 10% higher yield. On the other hand, a quarter of this load achieved the same performance in the temperature range 400-450 °C.

Overall, while thermodynamics predicts that higher conversions are expected for low temperature and high pressure, with a monotonous decrease of conversion with increasing temperature, the addition of kinetics clearly defines two distinct operating regimes. Under kinetic regime (before the maximum evidenced in Figures 5, 6, 10 and 11), an increase of temperature improves conversion, whereas after the maximum the system operates under thermodynamic regime, with decreasing conversion at increasing temperature. This transition temperature (that corresponding to the maximum, strictly depends on the operating pressure and reactants molar ratio.

3.4 Effect of cycle pressure

Restricting the analysis to the mixed catalyst layout (*i.e.* first bed of commercial iron-based catalyst plus one bed loaded with the ruthenium-based one) at the preferred reaction temperature of 430 °C, the effect of pressure on different outputs is shown in Figure . Actually, the only parameter appreciably affected by this variation is the compression duty needed to reach the desired operating pressure, while the total recycle flow depends essentially on the catalytic load (*i.e.* on the capability of the reactor to yield as much ammonia as the fresh feed at the highest possible concentration). The separation duty follows accordingly, since it is dominated by the latent heat of ammonia. For instance, the decrease of the operating pressure from 125 to 100 bar can decrease the gross compressors duty by *ca*. 7%, computed as difference of the compressors block duty for the two cases.

3.5 Reactor thermal profile for multibed configurations

At this point, the analysis was extended varying the bed loadings, at the fixed working pressure of 100 bars and at variables inlet temperatures around the central value of 400 °C. The results are represented in Figure 131, that shows the thermal condition and ammonia concentration along the reactor axial coordinate (stages lengths: 8 m, 8 m and 4 m), supposing to load each bed with different amounts of a catalyst obeying to the different kinetics model as in Table . The inter-cooling exchangers were not modelled rigorously, because in this phase we were only interested in considering the fate of the reactant mixture and the amount of heat to be subtracted to lower the temperature to the desired set point. Further work will compare alternative options including the preheating of the reactant mixtures and the recovery of the available reaction heat to sustain energy production cycles (e.g a Rankine cycle) to partially sustain the compressors duty.

Cases 4 – 10 show how the catalyst loading must be increased, to achieve the same ammonia yield, when the reactor inlet temperature is relatively low respect to the activation energy of the Wustite-based material. Notice that the Ru-loaded section, instead, works essentially in the same way since the activation energy for this material is the half than for Fe-based samples.

Cases 21 – 22 represent a complementary comparison, showing how the substitution of Wustite with Ruthenium in the last stage effectively increases ammonia concentration in the recycled stream: in this case, the higher temperature reached after the first stage is due essentially to the decreased gross heat capacity of the flowing mixture, while in the last stage this phenomenon is also enhanced by the higher activity of the Ru-material when the *hydrogen* content is lower. The second stage works more or less in the same way because, for Iron-based catalysts, it is a higher *ammonia* content that limits the reaction rate, and then the effect of a reduced gas flow is roughly compensated.

More generally, in order to produce ammonia gradually along all the reactor profile, lower inlet temperatures are preferable if the heat released by the reaction can be exploited to overcome the

activation energy, and the activity of the Ruthenium catalyst towards ammonia-enriched mixtures can keep the reaction going on in the last stage.

On this basis, also a strategy for the catalyst economization can be sketched, relaxing the assumption of working with strictly adiabatic beds. If, for example, a first Wustite bed is operated adiabatically with an inlet temperature and catalyst load that grant a high activity (case #32), then a following bed of the same material would experience a too high ammonia content, while its exiting temperature would yet be enough to keep an *isothermal* Ru-loaded bed active. Case #35 shows how a similar performance can be reached, with much less Wustite and more Ruthenium-based material, if the temperature profile of the reactor is properly managed: in case 38 this strategy is furtherly worked out in order to achieve a still reasonable ammonia concentration with (ideally) as little Ruthenium-based catalyst as possible. Then, only the final stages have to be loaded with Ruthenium, and their performance maximized if a *temperature decrease* (leading towards better equilibrium conditions, once the great part of the ammonia was produced), rather than adiabatic operation, can be assured. This assumption is probably the one that needs more development in further works. Nevertheless a similar management of ammonia reactor is not entirely new nor unfeasible [39–41], while other studies report at least a flat temperature profile as a better choice for the final stages [42].

Some computational details are reported for the interested reader in the Supplementary Information file.

4 Conclusions

A detailed study of the ammonia reaction yield with newly available kinetic and thermodynamic parameters was performed. The previously developed kinetic models for Ru/C, Fe-magnetite and Fe-wustite based catalysts were adapted for use in the Aspen Plus® plug flow reactor model. The preliminary validation of the calculations against the available experimental data was done to check

consistency and to assess the best operating conditions for each material. The best conditions for the single-pass operation of the Ru/C material were selected in the 400 – 450 °C range.

A multibed reactor configuration, with intercooling, was selected, holding different catalyst amounts and types. Mixing initial iron-based catalysts in the first bed(s) with Ru-based catalyst in the last one(s) revealed the best option to improve the yield with optimised catalyst loading. Accordingly, less demanding operating conditions can be envisaged for mixed multibed configurations.

List of acronyms and symbols

GHSV	Gas Hourly Space Velocity	η	Conversion
RPlug	Plug-flow reactor	k_0	Kinetic prefactor
RGibbs	Reactor for minimum Gibbs energy	K	Equilibrium constant
EOS	Equation Of State	P	Pressure
a	Activity	r	Reaction rate
Δ	Matrix determinant	R	Gas constant
E_a	Activation energy	s	Split fraction
f	Fugacity	T	Temperature
F	Mass flow	τ	Contact time

References

[1] Z.L. Zhu,, D.L. Chen, Nutr. Cycl. Agroecosystems 63(2–3) (2002) 117–27. 10.1023/A:1021107026067.

[2] P. Potter,, N. Ramankutty,, E.M. Bennett,, S.D. Donner, Earth Interact. 14(2) (2010). 10.1175/2009EI288.1.

[3] M. Reese,, C. Marquart,, M. Malmali,, K. Wagner,, E. Buchanan,, A. McCormick,, E.L. Cussler, Ind. Eng. Chem. Res. 55(13) (2016) 3742–50. 10.1021/acs.iecr.5b04909.

[4] T. Kandemir,, M.E. Schuster,, A. Senyshyn,, M. Behrens,, R. Schlögl, Angew. Chemie - Int. Ed. 52(48) (2013) 12723–6. 10.1002/anie.201305812.

[5] N. Cherkasov,, A.O. Ibhadon,, P. Fitzpatrick, Chem. Eng. Process. Process Intensif. 90 (2015) 24–33. 10.1016/j.cep.2015.02.004.

[6] R. Lan,, J.T.S. Irvine,, S. Tao, Int. J. Hydrogen Energy 37(2) (2011) 1482–94. 10.1016/j.ijhydene.2011.10.004.

[7] M.I. Temkin,, V. Pyzhev, Acta Physicochim. URSS (12) (1940) 327–56.

[8] L.J. Gillespie,, J.A. Beattie, Phys. Rev. (36) (1930) 743–53.

[9] L. Forni,, N. Pernicone, Catalysts for ammonia synthesis. PCT Int. Appl.(2003) WO 2002-EP11707 20021018, 2002.

[10] B. Lin,, Y. Qi,, Y. Guo,, J. Lin,, J. Ni, Catal. Sci. Technol. 5 (2015) 2829–38. 10.1039/C5CY00014A.

[11] M. Karolewska,, E. Truszkiewicz,, B. Mierzwa,, L. Keopiński,, W. Raróg-Pilecka, Appl. Catal. A Gen. 445–446 (2012) 280–6. 10.1016/j.apcata.2012.08.028.

[12] C. Fernández,, C. Pezzotta,, E.M. Gaigneaux,, N. Bion,, D. Duprez,, P. Ruiz, Catal. Today 251

(2015) 88–95. 10.1016/j.cattod.2014.11.010.

[13] K. Narasimharao,, P. Seetharamulu,, K.S. Rama Rao,, S.N. Basahel, J. Mol. Catal. A Chem. 411 (2015) 157–66. 10.1016/j.molcata.2015.10.019.

[14] J. Roman, Appl. Catal. A Gen. 400 (2011) 48–53. 10.1016/j.apcata.2011.04.010.

[15] D. Carpenter,, K. Maloney, System and method for ammonia synthesis. US9272920B2, 2012.

[16] B. Lin,, K. Wei,, J. Ni,, J. Lin, ChemCatChem 5(7) (2013) 1941–7. 10.1002/cctc.201200889.

[17] D.E. Brown,, T. Edmonds,, R.W. Joyner,, J.J. McCarroll,, S.R. Tennison, Catal. Letters 144(4) (2014) 545–52. 10.1007/s10562-014-1226-4.

[18] Z. Kowalczyk,, S. Jodzis,, W. Raróg,, J. Zieliński,, J. Pielaszek, Appl. Catal. A Gen. 173 (1998) 153–60. 10.1016/S0926-860X(98)00175-6.

[19] W.L. Luyben, Ind. Eng. Chem. Res. 49 (2010) 6150–63.

[20] É.S. Van-Dal,, C. Bouallou, J. Clean. Prod. 57 (2013) 38–45. 10.1016/j.jclepro.2013.06.008.

[21] D.-H. Jang,, H.-T. Kim,, C. Lee,, S.-H. Kim, Int. J. Hydrogen Energy 38(14) (2013) 6021–6. 10.1016/j.ijhydene.2013.01.167.

[22] M.B. Nikoo,, N. Mahinpey, Biomass and Bioenergy 32(12) (2008) 1245–54. 10.1016/j.biombioe.2008.02.020.

[23] S. Srinivas,, S.M. Mahajani,, R.K. Malik, Ind. Eng. Chem. Res. 49(20) (2010) 9673–92. 10.1021/ie100108p.

[24] M. Khoshnoodi,, Y.S. Lim, Fuel Process. Technol. 50(2–3) (1997) 275–89. 10.1016/S0378-3820(96)01079-X.

[25] A. Tripodi,, M. Compagnoni,, R. Martinazzo,, G. Ramis,, I. Rossetti, Catalysts 7(5) (2017). 10.3390/catal7050159.

[26] B.Y. Yu,, I.L. Chien, Ind. Eng. Chem. Res. 54(41) (2015) 10073–87. 10.1021/acs.iecr.5b02345.

[27] A. Aráujo,, S. Skogestad, Comput. Chem. Eng. 32 (2008) 2920–32. 10.1016/j.compchemeng.2008.03.001.

[28] P. Arora,, A.F.A. Hoadley,, S.M. Mahajani,, A. Ganesh, Ind. Eng. Chem. Res. 55(22) (2016) 6422–34. 10.1021/acs.iecr.5b04937.

[29] J. Andersson,, J. Lundgren, Appl. Energy 130 (2014) 484–90. 10.1016/j.apenergy.2014.02.029.

[30] I. Rossetti,, N. Pernicone,, L. Forni, Catalysis Today, Vol. 102–103, 2005, pp. 219–24.

[31] N. Pernicone,, F. Ferrero,, I. Rossetti,, L. Forni,, P. Canton,, P. Riello,, G. Fagherazzi,, M. Signoretto,, F. Pinna, Appl. Catal. A Gen. 251(1) (2003) 121–9. 10.1016/S0926-860X(03)00313-2.

[32] I. Rossetti,, L. Forni, Appl. Catal. A Gen. 282(1–2) (2005) 315–20.

[33] I. Rossetti,, N. Pernicone,, F. Ferrero,, L. Forni, Ind. Eng. Chem. Res. 45(12) (2006) 4150–5.

[34] I. Rossetti,, F. Mangiarini,, L. Forni, Appl. Catal. A Gen. 323 (2007) 219–25.

[35] D.C. Dyson,, J.M. Simon, Ind. Eng. Chem. Fundam. 7(4) (1968) 605–10. 10.1021/i160028a013.

[36] J.R. Jennings, Catalytic Ammonia Synthesis, Springer, Boston, 1991.

[37] H. Liu, Ammonia Synthesis Catalysts. Innovation and practice, Chemical Industry Press, 2013.

[38] B. Evans,, S. Hawkins,, G. Schulz ed., Ullmann's Encyclopedy of Industrial Chemistry, VCH, Weinheim, 1991.

[39] L.M. Patnaik,, I.G. Sarma,, N. Viswanadham, Int. J. Syst. Sci. 10(2) (1979) 225–41.

10.1080/00207727908941577.

[40] B. V. Babu,, R. Angira, Comput. Chem. Eng. 29(5) (2005) 1041–5. 10.1016/j.compchemeng.2004.11.010.

[41] D. Yancy-Caballero,, L.T. Biegler,, R. Guirardello, Chem. Eng. Trans. 43 (2015) 1297–302. 10.3303/CET1543217.

[42] N. Nikačević,, M. Jovanović,, M. Petkovska, Chem. Eng. Res. Des. 89(4) (2011) 398–404. 10.1016/j.cherd.2010.08.011.

[43] J. Ni,, J. Lin,, X. Wang,, B. Lin,, J. Lin,, L. Jiang, ChemistrySelect 2(21) (2017) 6040–6. 10.1002/slct.201700859.

[44] J. Ni,, R. Wang,, F. Kong,, T. Zhang,, J. Lin,, B. Lin,, K. Wei, Cuihua Xuebao 32(3) (2011) 436–9. 10.1016/S1872-2067(10)60179-9.

[45] D. Szmigiel,, W. Raróg-Pilecka,, E. Miśkiewicz,, M. Gliński,, M. Kielak,, Z. Kaszkur,, Z. Kowalczyk, Appl. Catal. A Gen. 273(1–2) (2004) 105–12. 10.1016/j.apcata.2004.06.020.

[46] C.A. Vancini, La sintesi dell'Ammoniaca, Hoepli, Milan, 1961.

Tables and Figures

Rate Expression	**Equation (2) (Ru/C)**				**Equation (5) (Wustite)**				**Equation (5) (Magnetite)**				**Equation (6) ('KM' Iron-based)**			
Stoichiometry	N_2		H_2	NH_3	N_2		H_2	NH_3	N_2		H_2	NH_3	N_2		H_2	NH_3
	-0.5		-1.5	1	-0.5		-1.5	1	-0.5		-1.5	1	-0.5		-1.5	1
Kinetic constant	E_a (kcal mol^{-1})		k_0 (kmol sec^{-1} kg^{-1}_{cat})		E_a (kcal mol^{-1})		k_0 (kmol sec^{-1} kg^{-1}_{cat})		E_a (kcal mol^{-1})		k_0 (kmol sec^{-1} kg^{-1}_{cat})		E_a (kcal mol^{-1})		k_0 (kmol sec^{-1} kg^{-1}_{cat})	
	23.0		426		45		7.47×10^8		47.5		3.23×10^9		40.76		1.72×10^8	
Rate Expression																
Exponents	N_2		H_2	NH_3	N_2		H_2	NH_3	N_2		H_2	NH_3	N_2		H_2	NH_3
Forward term (ν_r)	0.5		0.375	-0.25	1		2.25	-1.5	1		2.25	-1.5	1		1.5	-1
Reverse term (ν_p)	0		-1.125	0.75	0		-0.75	0.5	0		-0.75	0.5	0		-1.5	1
Coefficients	A	B	C	D	A	B	C	D	A	B	C	D	A	B	C	D
Term 1 (K_{for})	-7.19	0	0	0	-7.8	9218	-5.42	7.8×10^{-4}	-7.8	9218	-5.42	7.8×10^{-4}	-4.9	9218	-5.42	7.8×10^{-4}
Term 2 (K_{rev})	-1.876	-4609	2.69	1.27×10^{-4}	2.88	0	0	0	2.88	0	0	0	5.76	0	0	0
Adsorption Term																
Exponents	N_2		H_2	NH_3	na				na				na			
Term 1 (ν_i)	0		0	0												
Term 2 (ν_i)	0		0.3	0												
Term 3 (ν_i)	0		0	0.2												
Coefficients	A	B	C	D												
Term 1 (K_i)	0	0	0	0												
Term 2 (K_i)	-10.3	4529	0	0												
Term 3 (K_i)	-6.48	3523	0	0												

Table 1. Thermodynamic and kinetic parameters for the reaction models according to the Aspen Plus© formulation (8), where the equilibrium constants are expanded as: $ln(K) = A + B/T + C\times ln(T) + D\times T$.

Catalyst	T (°C)	P (bar)	GHSV (h^{-1})	NH_3 vol%	NH_3 Productivity (kg h^{-1} dm^3_{cat})	Reference
Ba-K-Ru/C	400	100	10000	20	1.5	[43]
Mg-Ba-Ru/C	400	100	10000	21	1.6	[44]
K-Cs-Ba-Ru/C	430	100	50000	14.1	5.3	[33]
Ba-Ru/MgO	400	90	-	11	-	[45]

Table 2. Comparison of different Ru-based catalysts performance.

Case #	P (bar)	Tin (°C)	Bed 1			Bed 2			Bed 3			Separator Duty (kW)	NH_3 max fraction (mol/mol)
			Catalyst Load (kg)	Kinetic model (Eq. n°)	Temperature profile	Catalyst Load (kg)	Kinetic model (Eq. n°)	Temperature profile	Catalyst Load (kg)	Kinetic model (Eq. n°)	Temperature profile		
4	100	430	10	(5)	Adiabatic + intercooling	10	(5)	Adiabatic + intercooling	5	(2)	Adiabatic + intercooling	206	9.56 %
10	100	400	15	(5)	Adiabatic + intercooling	15	(5)	Adiabatic + intercooling	10	(2)	Adiabatic + intercooling	196	9.66 %
21	100	400	20	(5)	Adiabatic + intercooling	20	(5)	Adiabatic + intercooling	20	(2)	Adiabatic + intercooling	151	13.2 %
22	100	400	20	(5)	Adiabatic + intercooling	20	(5)	Adiabatic + intercooling	20	(5)	Adiabatic + intercooling	237	7.47 %
32	100	430	10	(5)	Adiabatic + intercooling	10	(5)	Adiabatic + intercooling	10	(2)	Constant at inlet Temp.	155	12.4 %
35	100	400	5	(5)	Adiabatic + intercooling	7	(2)	Imposed rise	10	(2)	Imposed fall	140	13.4 %
38	100	400	7	(5)	Adiabatic + intercooling	3	(2)	Imposed rise	7	(2)	Imposed fall	164	11.5 %

Table 3. Summary of the input specifications for the test-cases at variable catalysts mix. In any case the ammonia yield is of 56-57 kg/h and the total compression power of 69-70 kW. Equation (2) represent the Ru-based catalyst, equations (5) and (6) the newer magnetite / wustite or the older commercial Iron respectively.

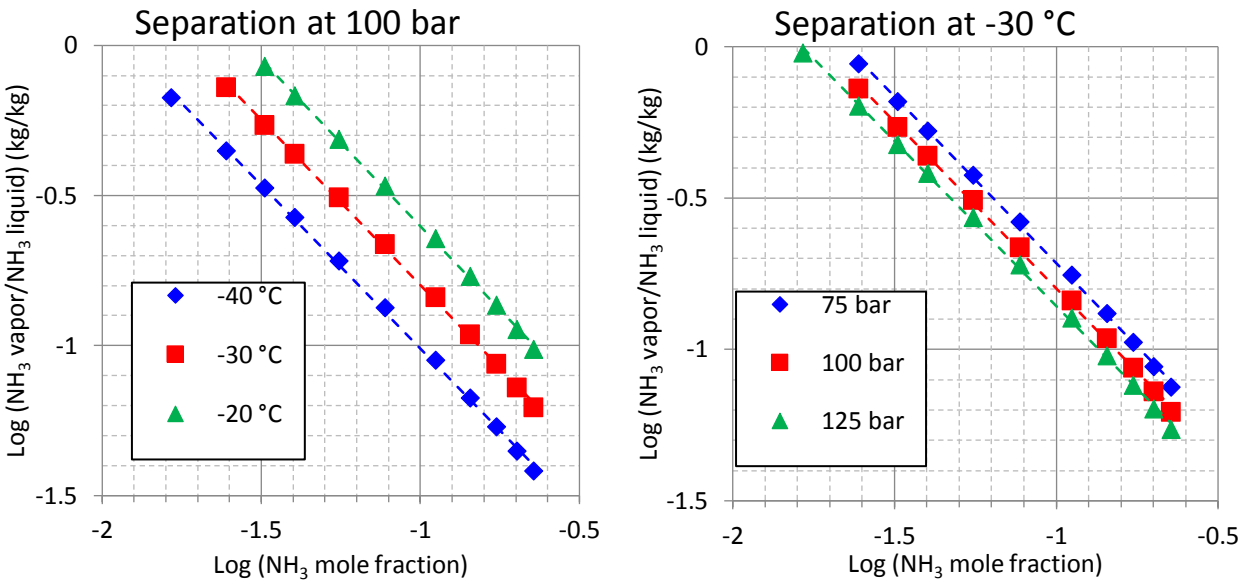

Figure 1: Vapor-liquid split fraction of ammonia in a stoichiometric H:N=3:1 (mol/mol) mixtures at equilibrium, calculated via the RKS-BM thermodynamic model. The dashed lines represents recognized power-law trends of the calculation.

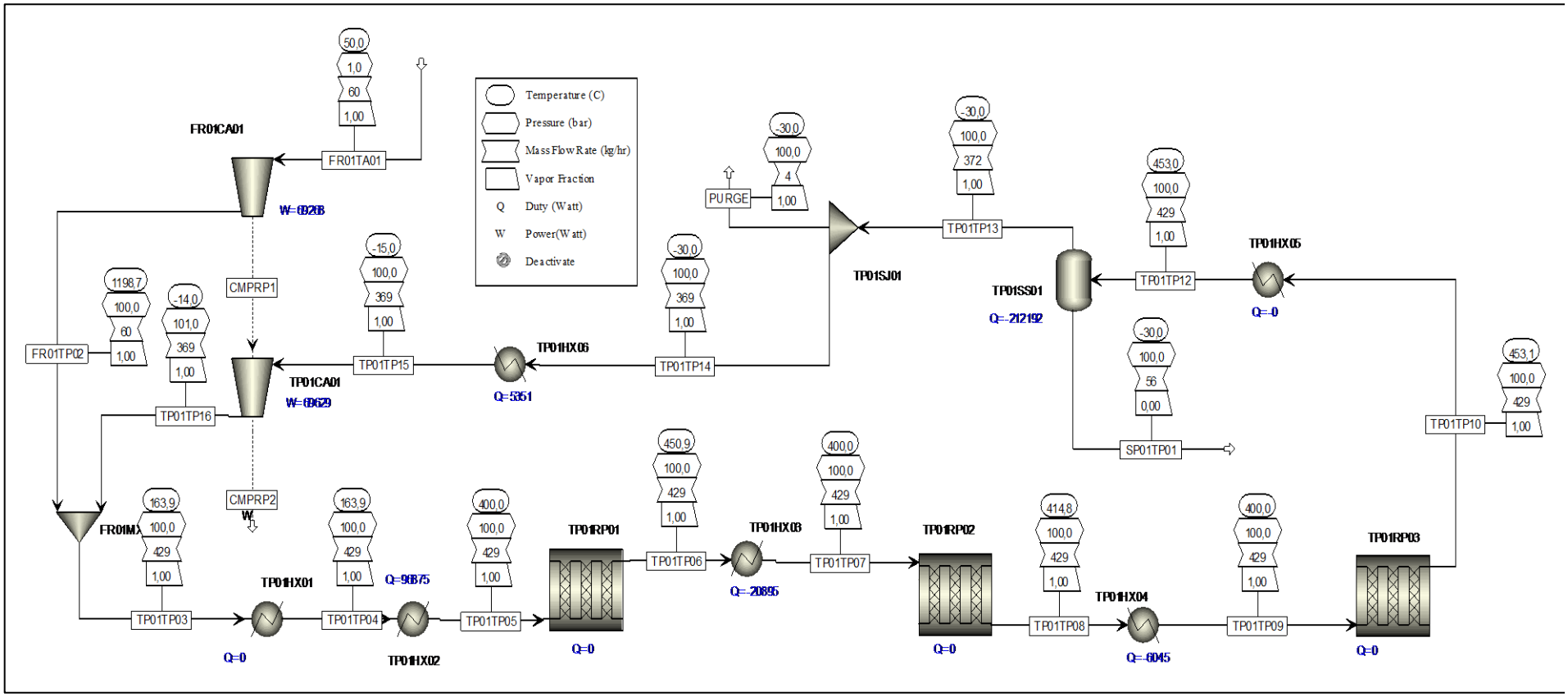

Figure 2: Basic layout employed for the simulation of an ammonia synthesis cycle [38,46]. The data are relative to a run of case 4 (Table) with a lower reactor inlet temperature.

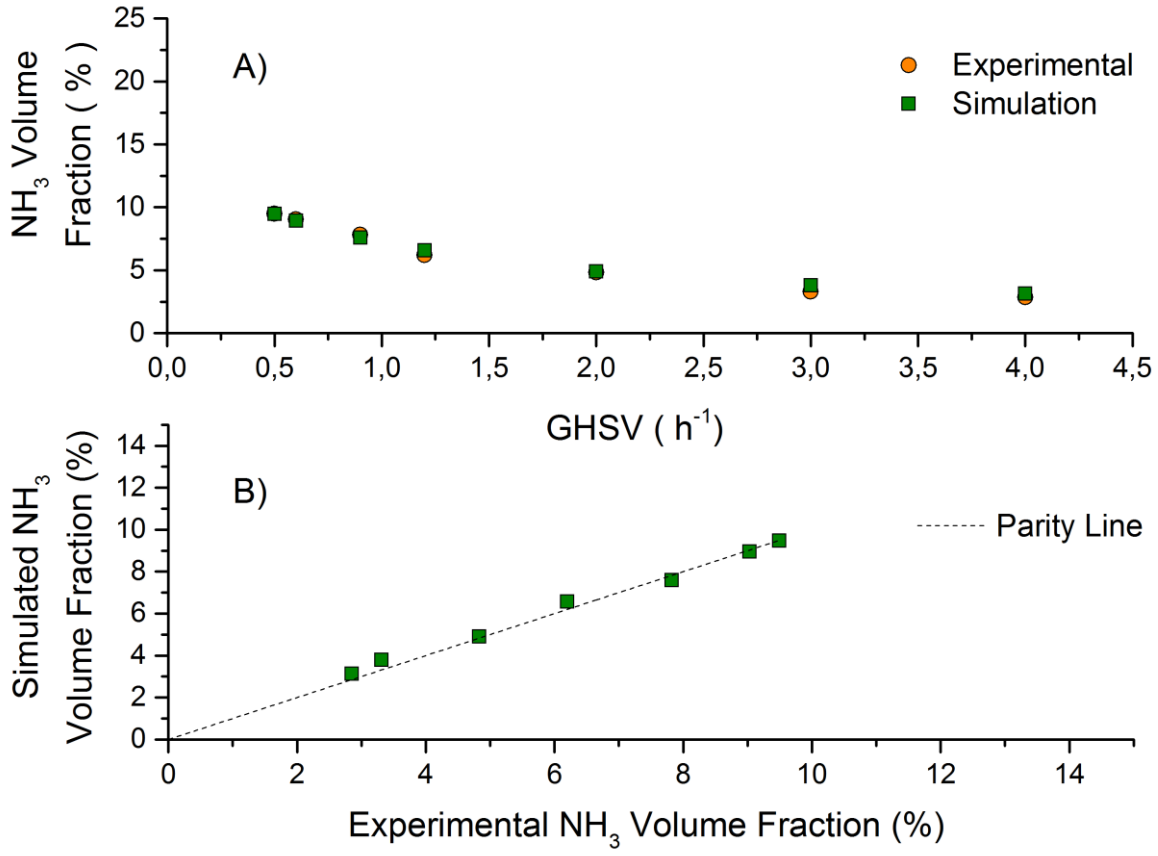

Figure 3: A) Example of data simulation for test at T = 430°C, P = 70 bar and H_2/N_2 = 1.5 (v/v). Experimental points (orange circles), simulated values (green squares). B) Parity plot.

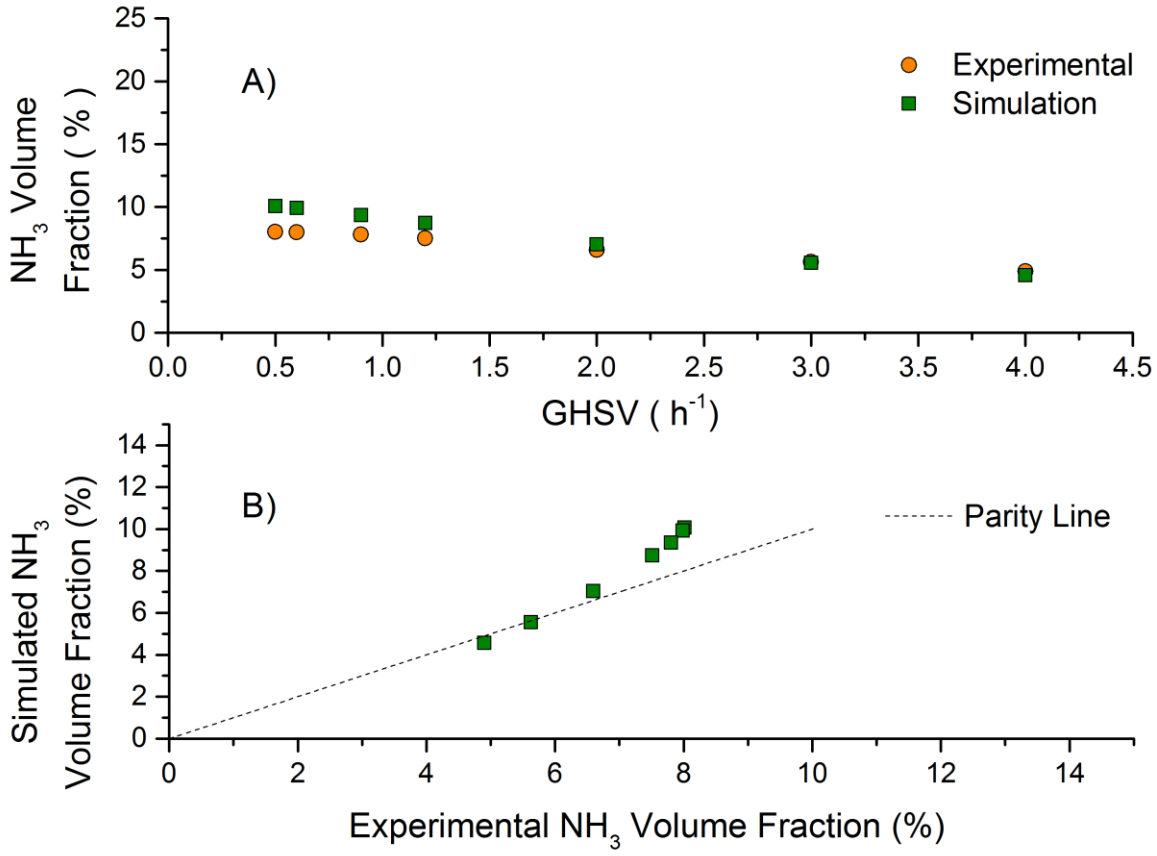

Figure 4: A) Example of data simulation for test at T = 460°C, P = 70 bar and H_2/N_2 = 1.5 (v/v). Experimental points (orange circles), simulated values (green squares). B) Parity plot.

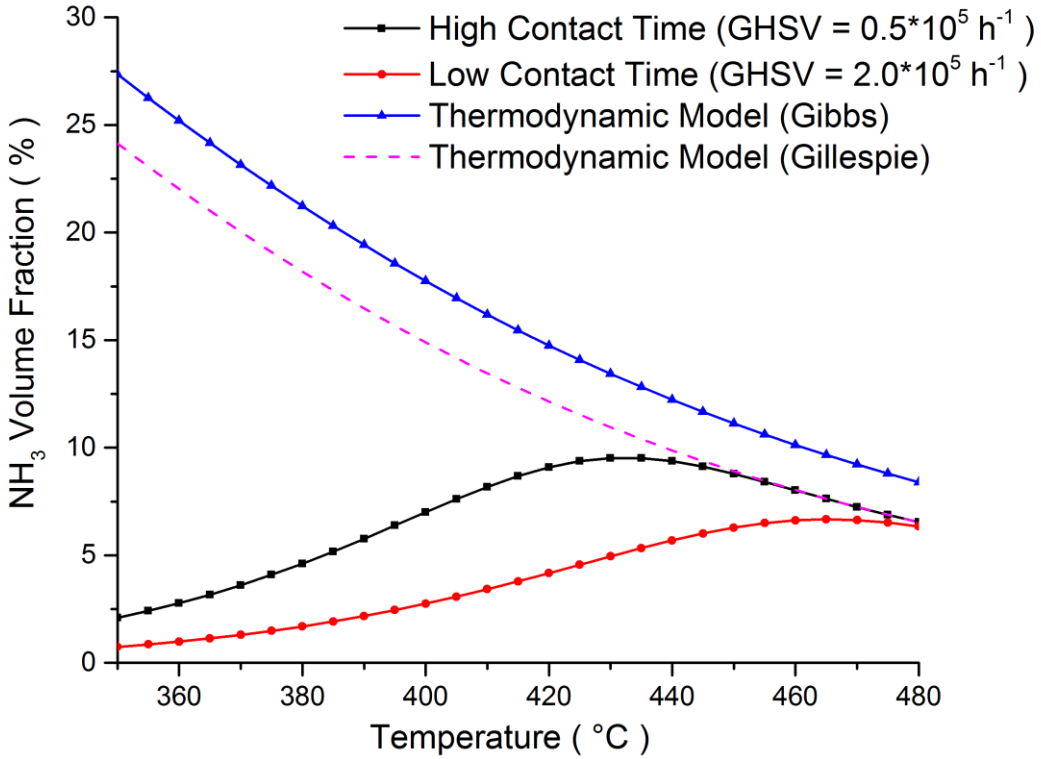

Figure 5: Comparison of ammonia production predicted by the here proposed kinetic model at low and high residence times (GHSV = 2.0×10^5 h^{-1} and 0.5×10^5 h^{-1}, respectively) and thermodynamic model under isothermal condition (P = 70 bar, H_2/N_2 = 1.5 v/v), calculated using Gibbs reactor or the equilibrium constant adopted for the kinetic expression (Gillespie).

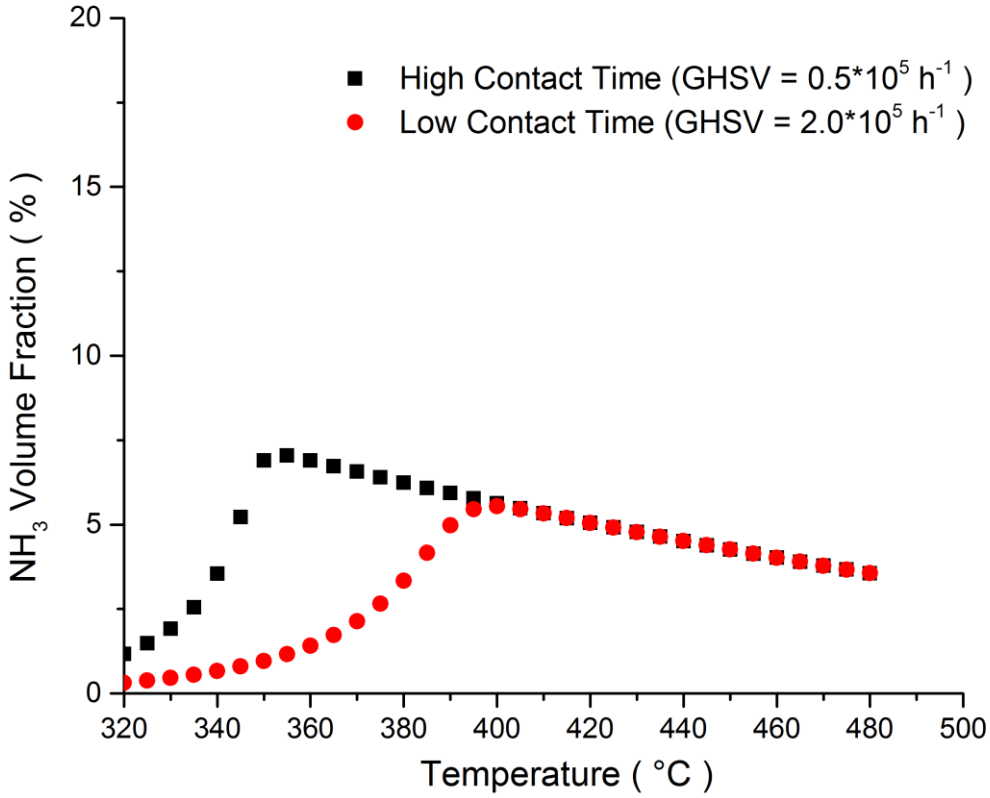

Figure 6: Comparison of ammonia production calculated by kinetic model (2) at low and high residence times (GHSV = $2.0*10^5$ h^{-1} and $0.5*10^5$ h^{-1} respectively) under adiabatic condition (P = 70bar, H_2/N_2 = 1.5 v/v), with respect to the reactor *inlet* temperature. The maxima of the isothermal analysis are anticipated since those thermal conditions are met, in this case, downstream along the reactor axis.

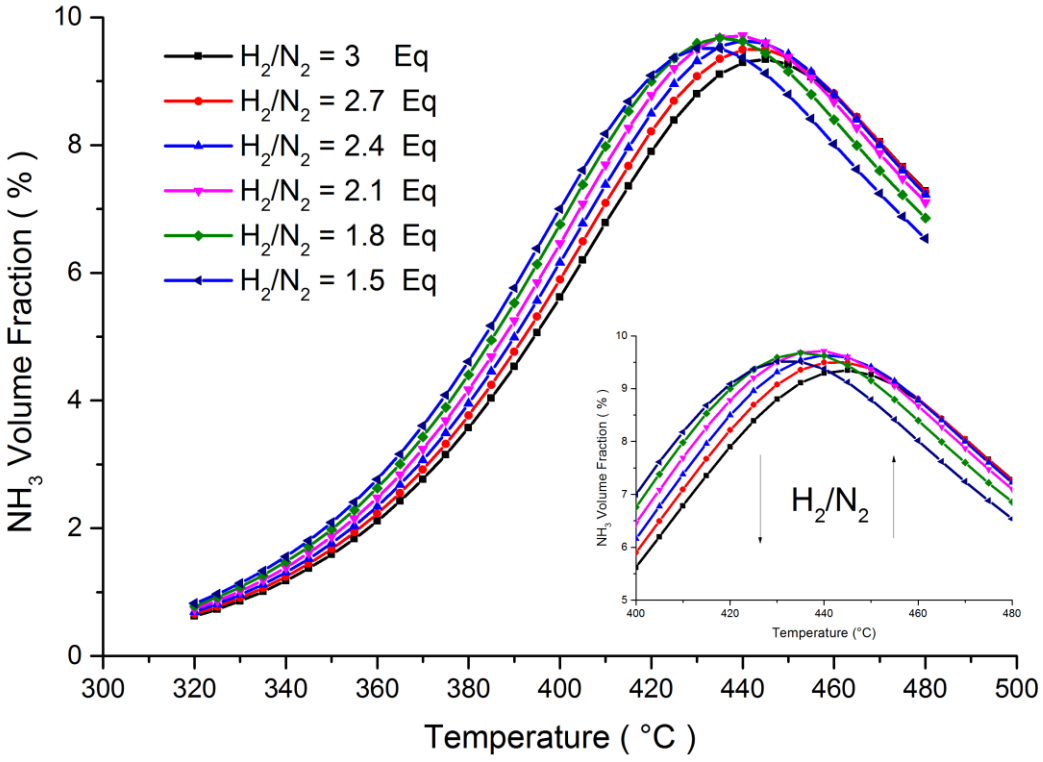

Figure 7: Comparison of ammonia production predicted by the kinetic model at different H_2/N_2 ratios GHSV = $0.5*10^5$ h^{-1} , P = 70bar).

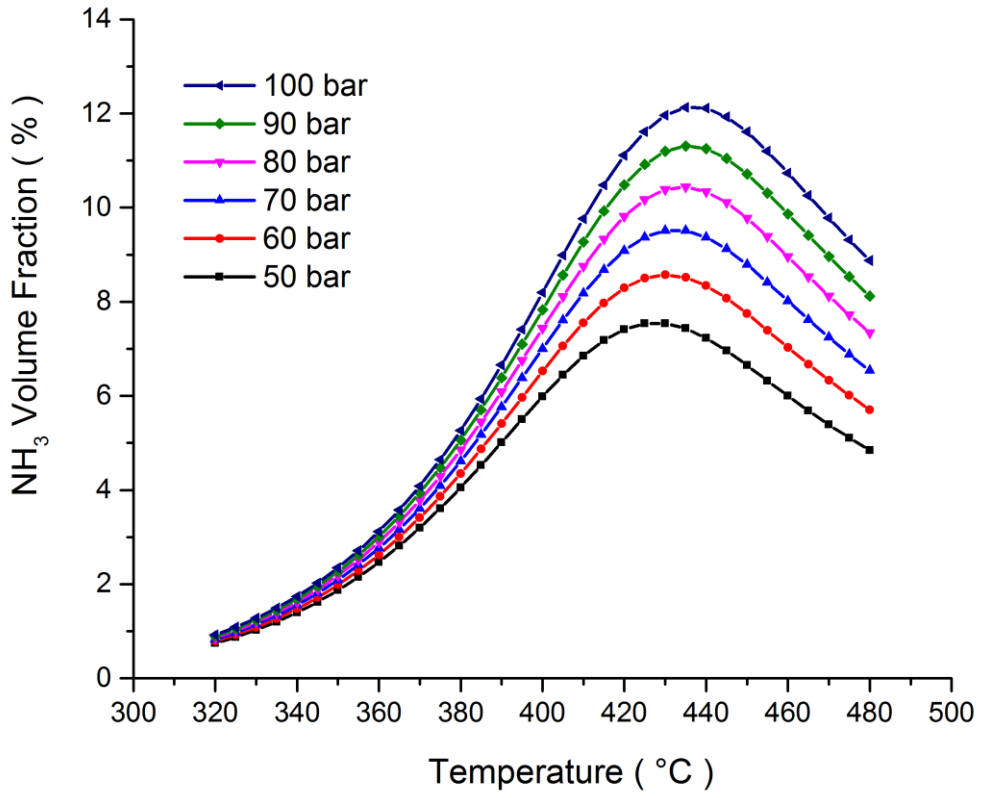

Figure 8: Comparison of ammonia concentration in the outlet gas predicted by the used kinetic model at different pressures (GHSV = $0.5*10^5$ h^{-1}, H_2/N_2 = 1.5 v/v).

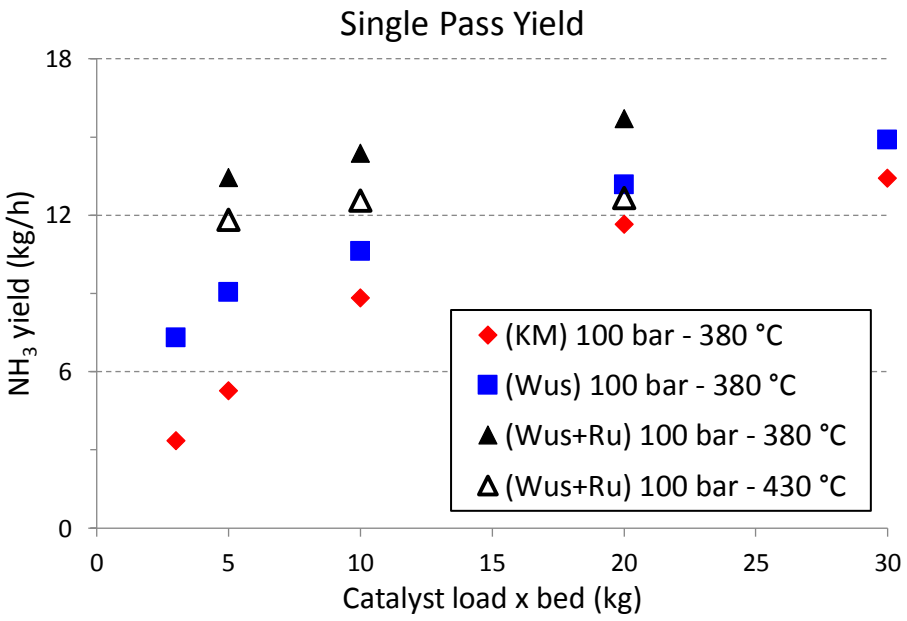

Figure 9: Open-loop comparison of the NH_3 yield for 3 adiabatic reaction beds, loaded each with the same amount of different catalysts and kept at the specified inlet temperature. 'KM'

catalyst is described by kinetic (6), while in simulation 'Wus' (for Wustite) and 'Ru' (Ruthenium) models (5) – (2) respectively are adopted.

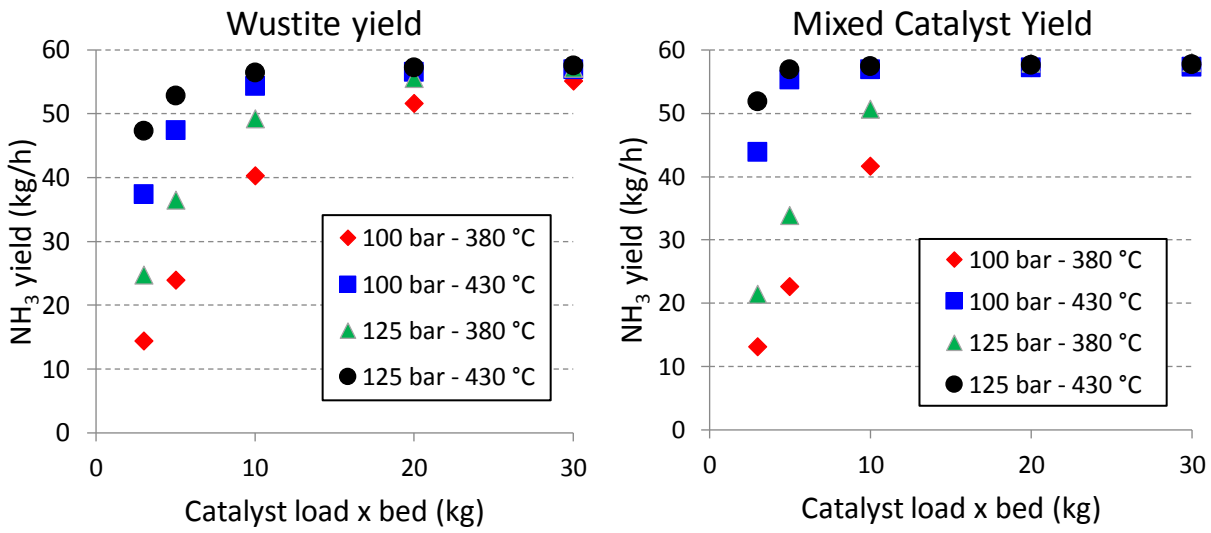

Figure 10: Closed-loop ammonia yields for 3 adiabatic reaction beds following model (5) (left) and models (5)-(5)-(2) (right) at the specified inlet temperatures and pressures.

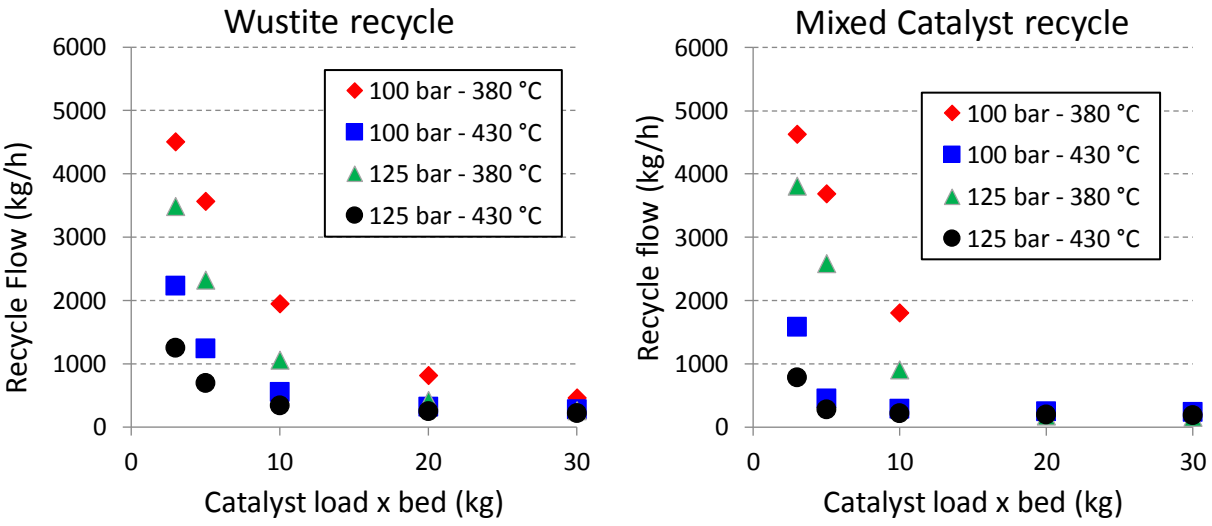

Figure 11: Closed-loop recycle flows for 3 adiabatic reaction beds following model (5) (left) and models (5)-(5)-(2) (right) at the specified inlet temperatures and pressures.

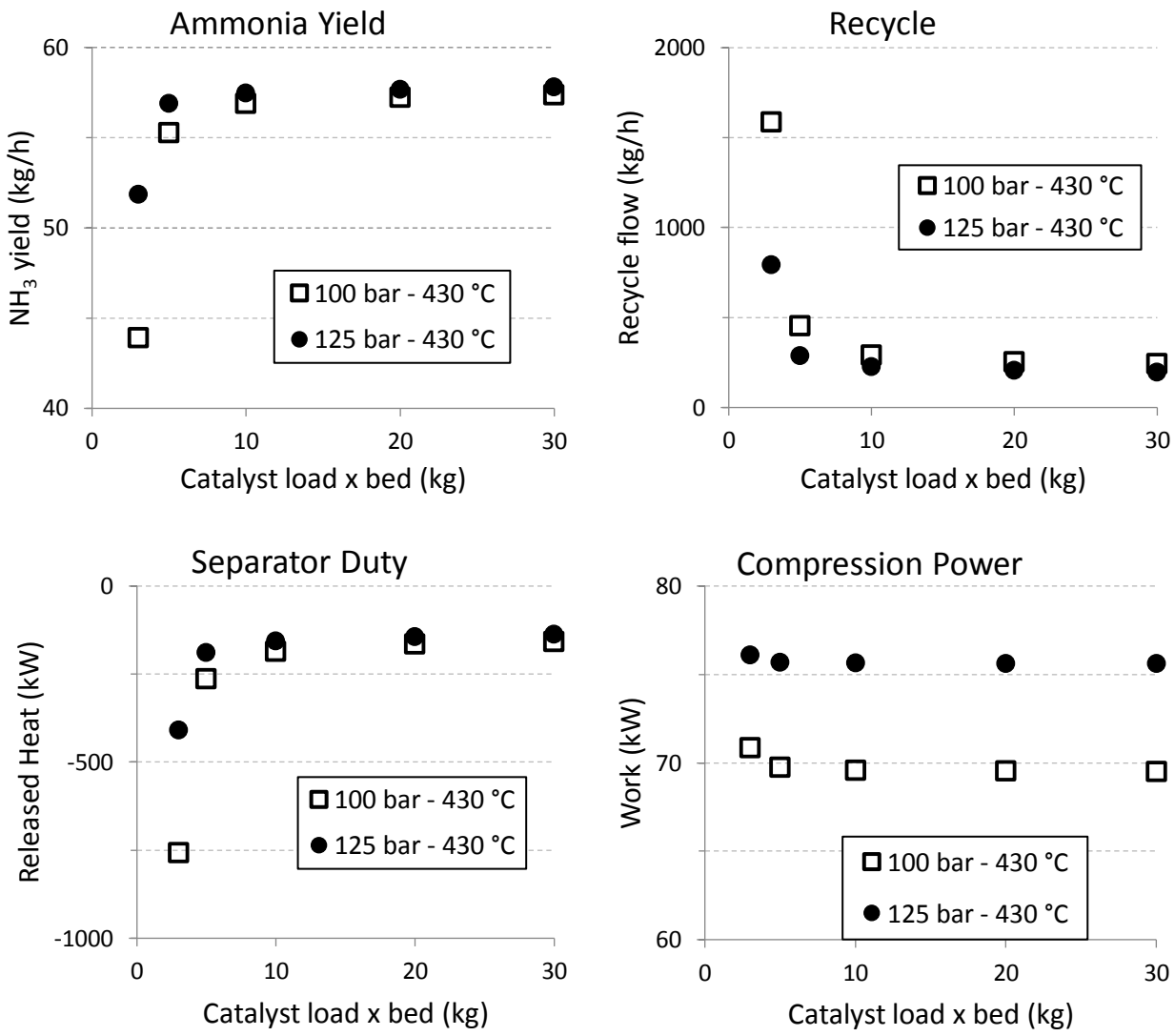

Figure 12: Closed-loop simulation results for 3 adiabatic reaction beds following the kinetic models (5)-(5)-(2) at the selected inlet temperature of 430 °C. The heat duties are negative as they represent released heat.

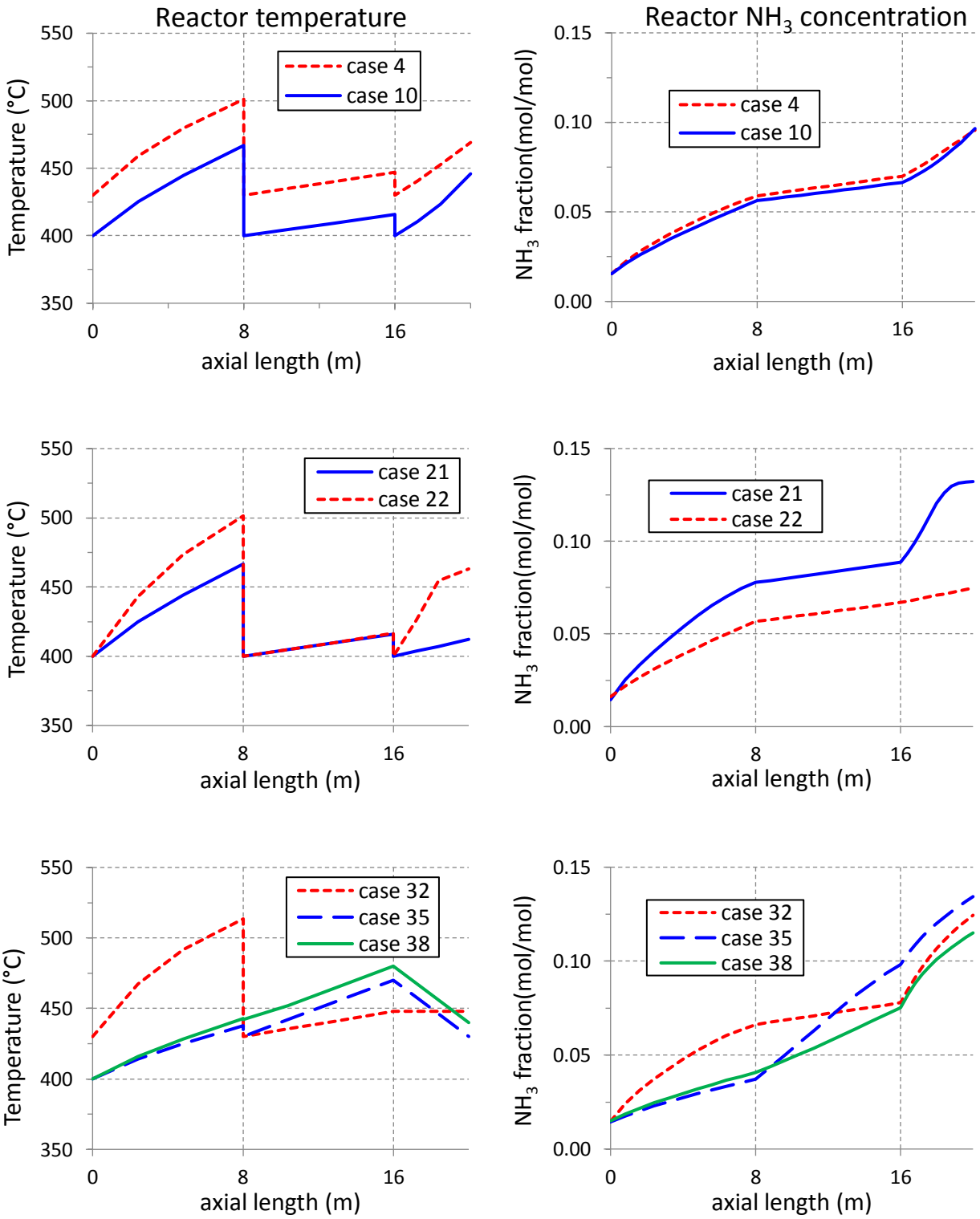

Figure 131: Reactor temperature and ammonia concentration for the closed-loop simulations summarized in Table .

Process simulation of ammonia synthesis over optimized Ru/C catalyst and multibed Fe + Ru configurations

Antonio Tripodi, Matteo Compagnoni, Elnaz Bahadori, Ilenia Rossetti†

Chemical Plants and Industrial Chemistry Group, Dip. Chimica, Università degli Studi di Milano, INSTM Unit Milano-Università and CNR-ISTM, via C. Golgi, 19, I-20133 Milano, Italy

Supplementary Information

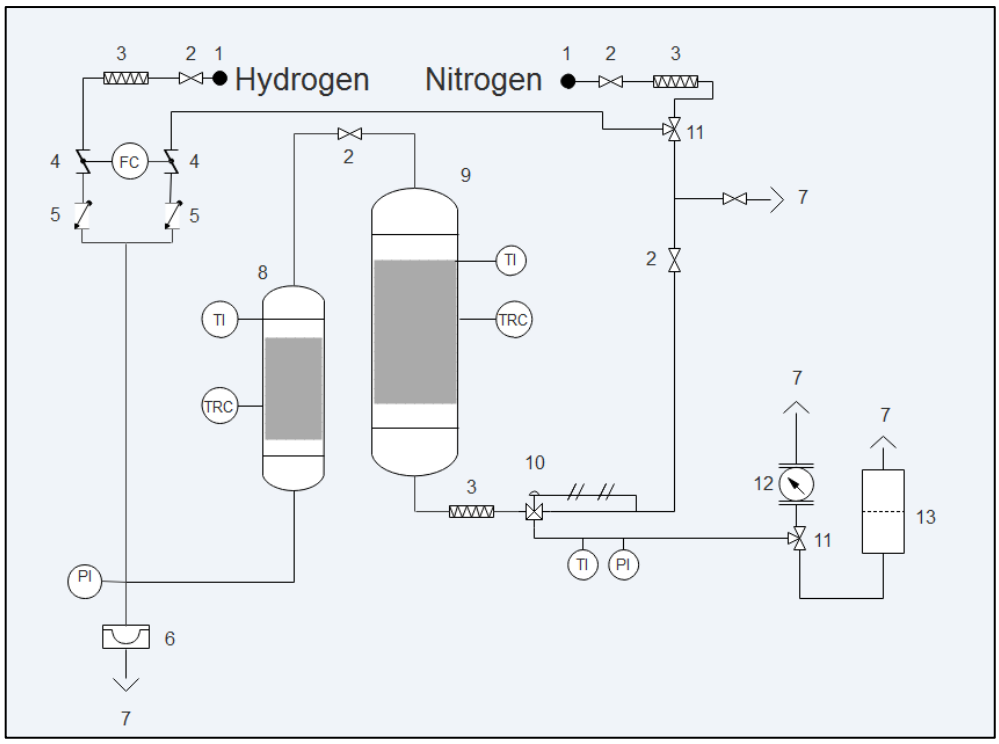

Figure S2: Scheme of the micro-pilot plant adopted. **1)** Inlet gas from cylinder; **2)** Shut off globe valve; **3)** Filter (2 μm); **4)** MSK mass flowmeter; **5)** non-return valve; **6)** Bursting disc; **7)** Vent; **8)** Chemical trap for possible poisons, containing an iron commercial catalyst coupled with eletric

† Corresponding author: ilenia.rossetti@unimi.it – fax: +39-02-50314300

oven; **9)** Testing reactor coupled with electric oven; **10)** PTFE-membrane relief valve; **11)** Three-way valve; **12)** Flowmeter; **13)** Chemical absorption trap for ammonia (H_2SO_4).

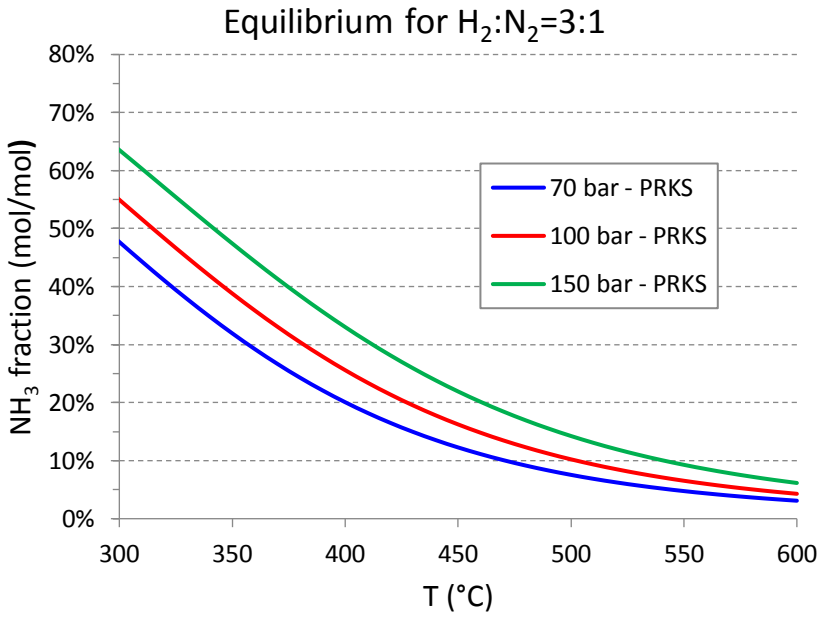

Figure S3: Equilibrium fractions for ammonia for a mixture containing 3 moles of hydrogen per mole of nitrogen at different pressures (in bar) – calculation performed minimizing the total Gibbs free energy with APV32 Pure-Component databanks and SRK equation of state data.

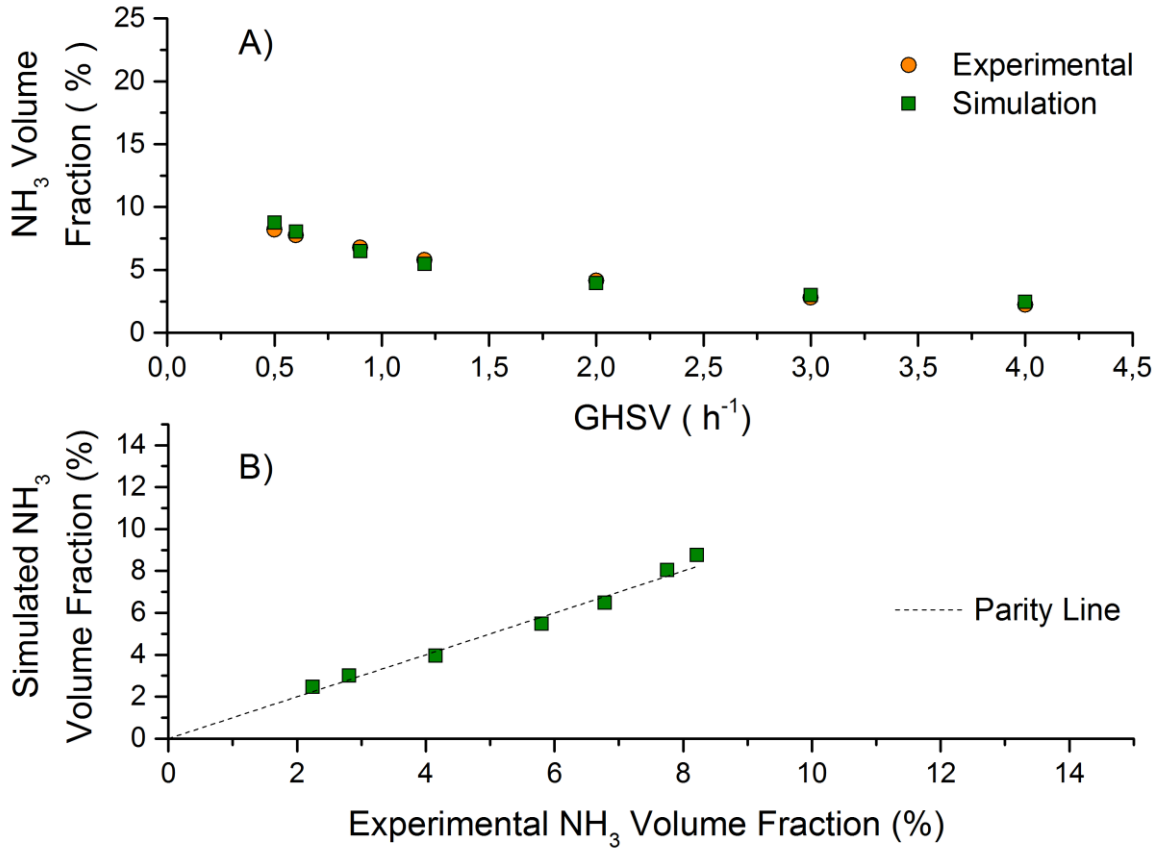

Figure S3: A) Example of data simulation for the test at T = 430°C, P = 70 bar and H_2/N_2 = 3 v/v. Experimental points (orange circles), simulated values (green squares). B) Parity plot for the outlet ammonia vol%.

A. Kinetic and Thermodynamic models

According to the reviewed literature, as summarized above, the gap between the intrinsic reaction kinetic and the whole process modelling is still to be fulfilled. The very example of ammonia process provided by Aspen Tech itself can be examined in this way: in fact, the reactor model resorts to an external subroutine, where many parameters are derived by plant experience and could be used only if they were derived for the same catalyst for whom the kinetic expression is given (see [1]. Notice, for example, that the expression of the rate upon a *volume* basis makes it hardly useful when void fractions, pellet sizes and bulk densities different from those of the referenced catalyst are considered, leaving the only tunable parameter 'catalyst activity' to be varied almost arbitrarily).

On the other hand, the overall mass balances rely on a separation block whose calculation was recently reassessed according to undisclosed plant data, that may be different from those used to adjust the kinetic subroutine. Moreover, it is altogether unclear whether the species' activities calculated by the recommended model (RKS-BM: Redlich-Kwong-Soave with Boston-Mathias modification) through the recycle line are coherent with those calculated by the kinetic subroutine formula: even if the reactor and separator blocks can be still considered reliable, (as long as they should reproduce *real* plant equipment), this poses at least a theoretical issue concerning the consistency of the overall calculation, especially because the recycle structure makes the outcome of one thermodynamic model to be influenced by the other's. Since in this work different intrinsic kinetics models are compared without attempting a detailed reactor' simulation (*i.e.* neglecting the corrections for the mass-transport phenomena), the review of the background thermodynamic was done on the separation section, and the same model used for the whole simulation. The recommended RKS-BM model was compared to the other commonly employed NRTL-RK system (Non-Random Two Liquid, also used in the same provided example in other blocks upstream) reproducing literature data [2–5] as reported in Figures S4 and S5 below. In general, the two systems behaves similarly reproducing the ternary NH_3-N_2-H_2 system (especially at higher pressures), while the NRTL-RK system returned better results evaluating the ammonia vapor fraction in more complex plant mixtures. Nevertheless, the RKS-BM package assures a fairly good calculation of the nitrogen and hydrogen vapor content, unlike the other. Considering that: *i)* the overall loop simulation is heavily influenced by the recycled vapor flow, but is much less sensitive to the ammonia residual fraction (see following section), and that *ii)* the 4-species mixture employed is not as demanding as the 5-chemicals system reviewed, the RKS-BM system was retained.

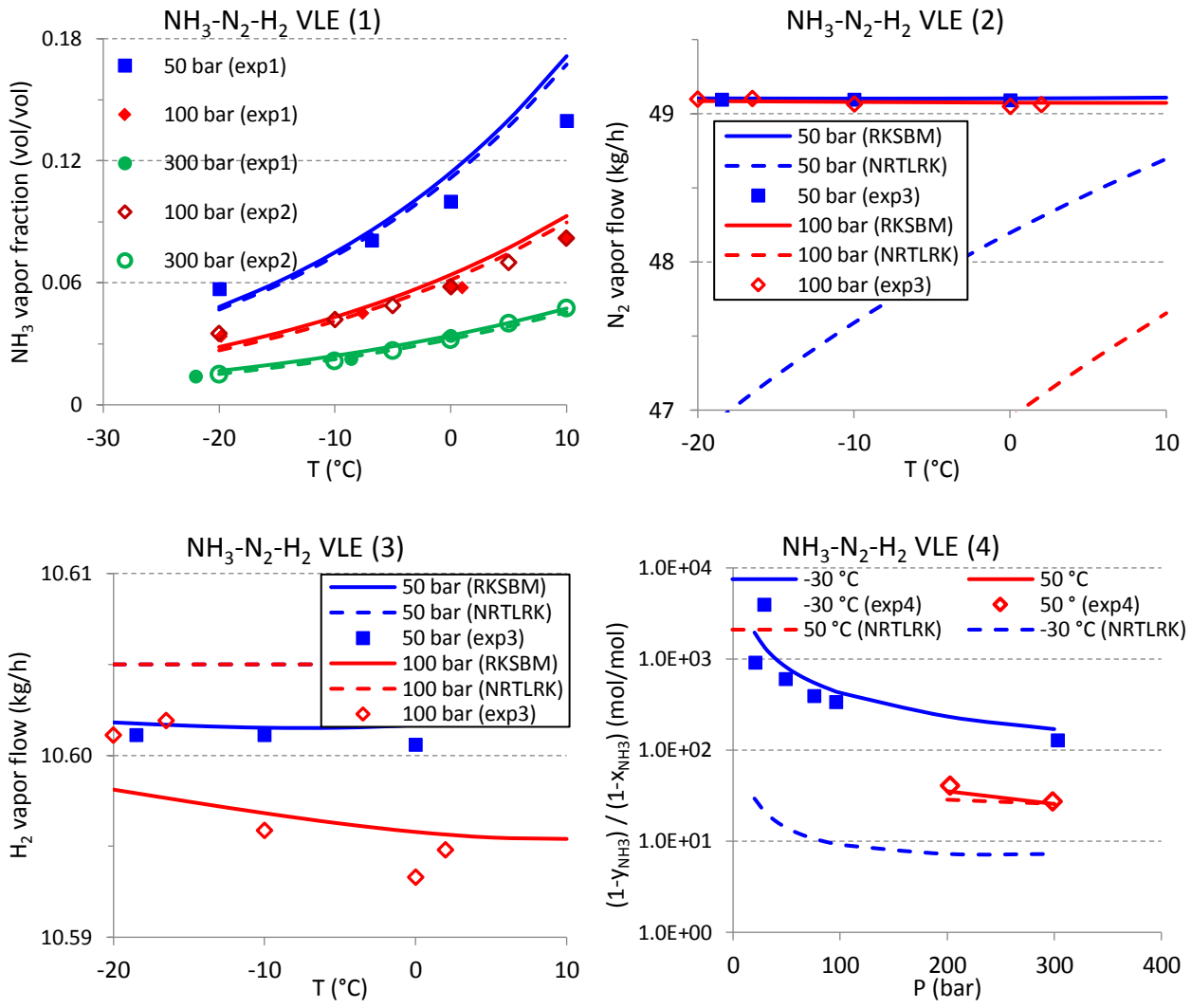

Figure S4: comparison between the RKS-BM calculation (solid lines) for a ternary mixture ammonia-nitrogen-hydrogen (30.0:49.1:10.6 kg/h) with liquid and vapor phases in equilibrium, the NRTL-RK one (dashed lines) and 4 different datasets: ‘exp1’ from [3], ‘exp2’-‘exp3’ from [2] and references therein, ‘exp4’ as reported in [5].

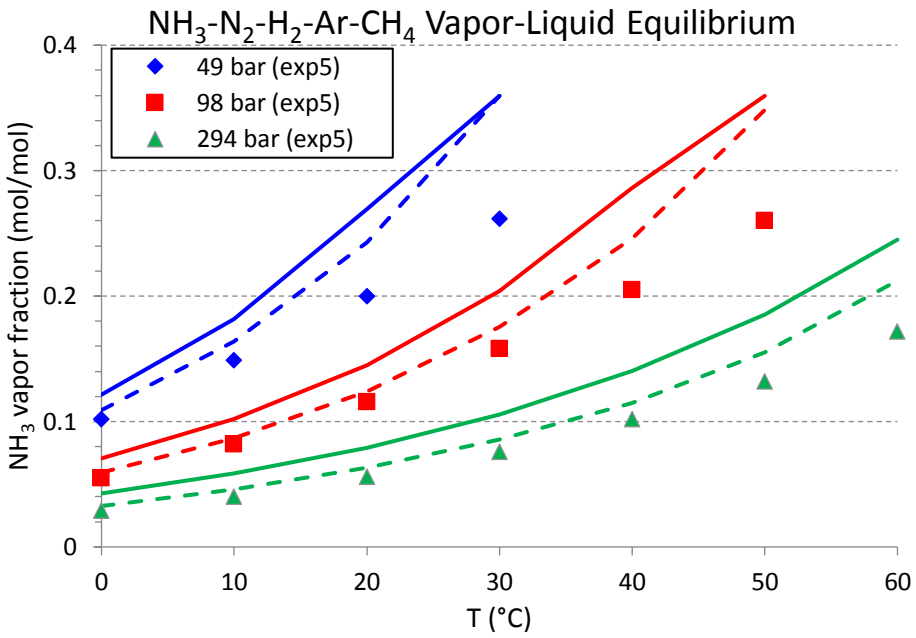

Figure S5: comparison between the RKS-BM calculation (solid lines) of the 5-species mixture ammonia-nitrogen-hydrogen-methane-argon (50.0:49.1:10.6:12.8:13.3 kg/h), the NRTL-RK one (dashed lines, same input) and dataset 'exp5' that reports plant data as found in [4].

B. Computational Details: Equilibrium Constant

The quadratic term reported in Eq. (7) was at first neglected according to Aspen Plus© format for the temperature dependence of equilibrium constants. An alternative strategy was to adjust the other terms so to reproduce the same $K_{eq}(T)$ function in the considered temperature range, leading to a slightly different expression with respect to the one reported in Table 1:

$$\ln K'_{eq} = +1.9 + \frac{4609}{T} - 2.71 * \ln T + 0.00039\,T$$

The adjustment was made minimizing the sum of the square differences: $\sum_i (K(T_i) - K'(T_i))^2$ via a Newton method implemented within the MS-Excel™ solver plug-in. Notice that Table 1 reports the coefficients with opposite sign, since the input form of Aspen Plus expects the inverse of the equilibrium constant.

C. Computational Details: Recycle Convergence

Despite its apparent simplicity, the coupled reactor–separator behavior hides tricky features that may not be handled correctly by the acceleration features of the default 'Wittig' convergence algorithm and prove difficult to solve even for the 'Broyden' method (a quasi-Newton one). Referring to the block scheme of Figure, denoting with *s* the fraction of any species recycled after the separator-purge and with *x* the amount of ammonia produced within the reactor, then the balances are expressed by 3 linear equations in the unknown flowrates *F*: $\underline{\underline{A}} \times \underline{F} = \underline{B}$ where:

$$\underline{\underline{A}}_{NH_3} = \begin{bmatrix} 1 & 0 & 1 \\ 1 & -1 & 0 \\ 0 & s_{NH_3} & -1 \end{bmatrix}, \qquad \underline{B}_{NH_3} = \begin{bmatrix} 0 \\ -x \\ 0 \end{bmatrix} \tag{S9}$$

$$\underline{\underline{A}}_{N_2} = \begin{bmatrix} 1 & 0 & 1 \\ 1 & -1 & 0 \\ 0 & s_{N_2} & -1 \end{bmatrix}, \qquad \underline{B}_{N_2} = \begin{bmatrix} n_0 \\ \frac{14}{17}x \\ 0 \end{bmatrix} \tag{S10}$$

$$\underline{\underline{A}}_{H_2} = \begin{bmatrix} 1 & 0 & 1 \\ 1 & -1 & 0 \\ 0 & s_{H_2} & -1 \end{bmatrix}, \qquad \underline{B}_{H_2} = \begin{bmatrix} h_0 \\ \frac{3}{17}x \\ 0 \end{bmatrix} \tag{S11}$$

with the column of every matrix representing the streams 1,2 and 3 of Figure S6, and n_0, h_0 are the fresh nitrogen and hydrogen makeup flowrates.

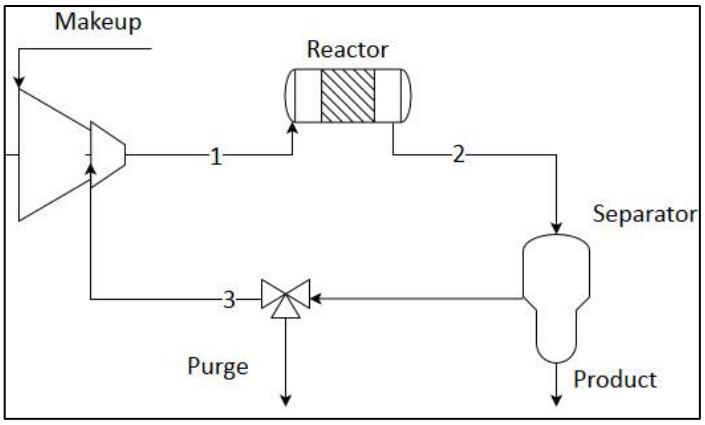

Figure S6: simple block-scheme of an ammonia synthesis cycle, used to write the 9-equations linear system [2,6].

The first issue of such a system is recognized as in any case: $\Delta_A = s(1-s)$, where *s* is actually much less than 1 only for ammonia. In other words, the recycled flows of nitrogen and hydrogen tends to diverge non-linearly as the purge fraction is decreased. This causes the 'Flash2' block to separate less liquid, since the thermodynamic model calculates a higher dew point as the mixture becomes richer in the non-condensable species, so the parameter *s* can decrease, between two simulation steps, even if the purge fraction is constant. Besides the inherent difficulty for the numerical methods to calculate the A^{-1} matrix as $\Delta \approx 0$, the convergence iterations may bring the succession $\Delta_k \rightarrow \Delta_{k+1}$ to approach 0 and the successions $F_k \rightarrow F_{k+1}, (F_{k+1} - F_k)_k$, to diverge. These combined features may result in: *i)* an earlier calculation error (if Δ is too little), *ii)* a tolerance error (typical for the Secant or Wittig algorithms as $\Delta F / F$ becomes too large), *iii)* a nested 'division-by-0' error (typical for the Newton method, sensitive to the derivative $\partial \Delta F / \partial F$) or *iv)* a 'flash-failure' error as the separator block cannot handle any liquid phase formation. Another numerical perturbation for the convergence steps lies in the nitrogen split fraction at the flash block, that varies according to the liquid phase formation.

A help to the system stability comes from the removal of hydrogen operated in the reactor, but this feature may not be sufficient if *i)* the ammonia fraction in the separator is still too low (and hence the liquid phase outflow cannot match the fresh feed inflow) or *ii)* the catalyst load is too low.

Also checking carefully the above system parametrization beforehand, the numerical stability of these closed-cycle simulation relies critically on the supposed purge fraction and a sound initial guess of the tear-stream exiting the reactor (shifting upwards the ammonia flow and downward the hydrogen one is often of help). Notice that purging a non-negligible gas flow of 1%, the value of Δ_A for hydrogen can be so low as to make tolerance warning or errors be issued, even if the reports are practically correct.

As an example, consider the simulations sequence reported in: the reactor calculation of the kinetic model (5) (for 3 adiabatic beds initially loaded with 3 kg of catalyst each, fed at 400 °C and 100 bar) yields *ca*. 9 kg/h of ammonia at open recycle. This result is used as the first guess for the reactor outlet stream in a semi-closed loop, whose result is in turn the first guess for a further calculation until the cycle is closed.

After every run the simulation results were reinitialized, to evaluate the convergence capability of the algorithm when it relies only on the controlled input represented by the tear-stream specification. Moreover, this option becomes mandatory when automated case-by-case simulations are planned, since the calculus is not much sensitive to the recirculating flow values of hydrogen and nitrogen and may fail to update them. The first convergence issue (between cases 6 and 7) reflects the sudden decrease of the calculated Δ as the purge fraction becomes low. Then, it can be noticed that the algorithm works better while coping with specie's build-up (case 9) than with specie's depletion (cases 10-11 and 12-13), which is due to the fact that the hydrogen removal within the liquid ammonia is always negligible respect to its removal at the purge. Nevertheless, cases 14-16 seem to show that the proper initialization of the tear stream is the most important procedure to adopt, since the same cycle conditions handled (yet not easily) in case 13 become troublesome to reach from different

starting points (even if already closer to the results): a more careful inspection of the simulation reports for case 14 (here not shown) indicates that the tear-stream last pass deviation $(F_{k+1} - F_k)$ is acceptable from a practical point of view, as confirmed by the results of the manual calculation (bracketed numbers, performed with Matlab®) using the values of *x* and *s* retrieved from the Aspen Plus blocks. In this case, the key to reorder the convergence is to surmise a *wrong* tear stream flow of Nitrogen (very sensitive to build-up like hydrogen, but on higher absolute values), which is most likely due to the oscillating behavior of the error that may spring from starting points too near to the results with this kinds of algorithms. The marked dependence of the tear convergence on a *suitable* (rather than *precise*) tear-stream initial guess, actually prevents the use of the automated 'sensitivity analysis' tool over a widespread range of system conditions.

As for the manual calculation correctness, it depends on the alignment of *s* and *x* to their realistic values, and has to be checked a-posteriori because these parameters are strongly non-linear functions of the species' flows (even at fixed temperature and pressure) and their explicit representation would turn the system into a non-linear one. It can be readily verified that the nitrogen vapor separation is the main issue of the iterative calculation: the bracketed results for case 14 were retrieved supposing a vapor/total N_2 fraction of 0.999 (kg/kg), while increasing this quantity by 0.1% (to 0.9999) the recycled flow increases by 20% (from 1099 to 1292), amounting to a sensitiveness of the order of 10^2.

These considerations help to clarify the choice of the RKS-BM method, as also shown by the test calculation sequence listed from case 17 onward. While cases 18-20 were tired just to check the already known tear-stream sensitiveness also with the NRTL-RK, the step between cases 17-18 and cases from 22 on confirm that the total recycle flow and the computational load are strongly influenced by the correct description of all the species present in the vapor phase: on this basis, the NRTL-RK model was put aside despite its better reproduction of the ammonia split.

Case	Purged vapor (kg/kg)	Tear stream Flow guess (kg/h)				Tear stream Flow results (kg/h)				Iterations	Converged
		N_2	H_2	NH_3	CH_4	N_2	H_2	NH_3	CH_4		
open	99%	-	-	-	-	41.2	8.89	10.1	0.283	4	yes
1	80%	41.2	8.89	10.1	0.283	50.0	10.8	11.5	0.350	6	yes
2	60%	50.0	10.8	11.5	0.350	65.6	14.2	13.0	0.465	8	yes
3	40%	65.6	14.2	13.0	0.46	96.5	20.8	15.4	0.697	10	yes
4	20%	96.5	20.8	15.4	0.697	184	39.8	21.4	1.39	13	yes
5	10%	184	39.8	21.4	1.39	348	75.1	31.3	2.77	15	yes
6	5%	348	75.1	31.3	2.77	656	141	47.6	5.52	21	yes
7	1%	656	141	47.6	5.52	2929	632	153	27.4	33‡	yes

‡ Convergence steps exceed the default value of 30.

8	0.5%	29 29	63 2	15 3	27.4	5695	12 29	27 8	54.8	23	yes
Inlet reactor Temperature lowered from 400 to 350 °C											
9	0.5%	56 95	12 29	27 8	54.8	8529	18 40	38 6	55.7	13	yes
Catalyst load increased to 10 kg x bed – 20 kg x bed											
10	0.5%	85 29	18 40	38 6	55.7	5712	12 32	27 9	54.8	22	yes
11	0.5%	57 12	12 32	27 9	54.8	2728	58 8	16 5	51.6	24	yes
Pressure decreased to 75 bar – increased to 125 bar											
12	0.5%	27 28	58 8	16 5	51.6	5949	12 83	34 3	55.1	26	yes
13	0.5%	59 49	12 83	34 3	55.1	1161	25 0	98. 9	43.8	41‡	yes
Pressure and Temperature restored to 100 bar – 400 °C											
13	0.5%	11 61	25 0	98. 9	43.8	417	89. 5	76. 6	32.7	30	yes
Catalyst load decreased to 10 kg x bed											
14	0.5%	41 7	89. 5	76. 6	32.7	(109 9)	(28 2)	(10 6)	-	55‡	no

15	0.5%	1181	254	106	45.2	1181	254	106	45.4	54‡	yes
16	0.5%	1200	250	100	40	1181	254	106	45.4	36‡	yes
17	1%	420	90	73	20	879	189	88.4	24.4	26	yes
Separation block model: NRTL-RK											
18	1%	879	189	88.4	24.4	558	238	85.3	7.78	43‡	yes
19	1%	600	200	80	5	-				27	no
20	1%	550	200	80	5	-				55‡	no
21	1%	500	200	80	5	558	238	85.3	7.77	43‡	yes
Separation block model: RKS-BM											
22	1%	500	200	80	5	-				55‡	no
23	1%	780	200	80	5	-				55‡	no
24	1%	500	150	80	5	-				55‡	no

25	1%	900	180	80	5	879	189	88.4	24.4	39‡	yes
26	0.5%	880	180	85	24	1180	255	106	45.5	45‡	yes

Table S1: test calculation sequence to check the recycle convergence performances (algorithm: Broyden, tolerance: 10^{-5}).

[1] (2008).

[2] C.A. Vancini, La sintesi dell'Ammoniaca, Hoepli, Milan, 1961.

[3] A.T. Larson,, C.A. Black, J. Am. Chem. Soc. 47(4) (1925) 1015–20. 10.1021/ja01681a014.

[4] K. V. Reddy,, A. Husain, Ind. Eng. Chem. Process Des. Dev. 19(4) (1980) 580–6. 10.1021/i260076a013.

[5] M.R. Sawant,, A.W. Patwardhan,, V.G. Gaikar,, M. Bhaskaran, Fluid Phase Equilib. 239(1) (2006) 52–62. 10.1016/j.fluid.2005.10.014.

[6] B. Evans,, S. Hawkins,, G. Schulz ed., Ullmann's Encyclopedy of Industrial Chemistry, VCH, Weinheim, 1991.